TABLE 3
Regression models for BEE and body composition and other clinical factors[1]

	Coef (95% CI)	SE	Std coef	*P*	Adjusted R^2
Model 1					
BEE (FFM + FM)					0.795
Intercept	400.0 (277.1, 523.1)	61.4	—	<0.001	
FFM	17.0 (14.3, 19.7)	1.3	0.83	<0.001	
FM	4.3 (0.3, 8.4)	2.0	0.14	0.038	
Model 2[2]					
BEE (FFM + FM + CPR6′ + INS + PR)					0.834
Intercept	256.2 (59.3, 453.0)	98.1	—	0.012	
FFM	16.9 (14.3, 19.4)	1.3	0.82	<0.001	
FM	5.8 (1.8, 9.8)	2.0	0.19	0.006	
CPR6′	−19.9 (−35.6, −4.1)	7.9	−0.16	0.015	
Insulin[2]	−69.9 (−124.0, −15.7)	27.0	−0.15	0.012	
PR	3.3 (0.8, 5.9)	1.3	0.15	0.011	

[1] Model 1 predicted BEE only from body composition by linear regression analysis (n = 58). The final regression model (model 2) used independent variables selected from FFM, FM, age, sex, CPR6′, fasting plasma glucose, mean preprandial plasma glucose, A_{1c}, dietary energy, use of insulin, use of metformin, use of sulfonylurea, and pulse rate by stepwise estimation (n = 58). A_{1c}, glycohemoglobin (%); BEE, basal energy expenditure (kcal/d); Coef, partial regression coefficient; CPR6′, C-peptide immunoreactivity 6 min after intravenous glucagon injection (ng/mL); FFM, fat-free mass (kg) measured by using dual energy X-ray absorptiometry; FM, fat mass (kg) measured by using dual energy X-ray absorptiometry (kg); INS, insulin; PR, pulse rate (beats/min); Std coef, standardized coefficient.
[2] Use = 1; nonuse = 0.

and use of metformin (r = 0.40). FPG had a negative correlation with the use of sulfonylurea (r = −0.36). Mean preprandial PG had a positive correlation with the use of insulin (r = 0.37) and a negative correlation with the use of metformin (r = −0.38). Insulin secretion (CPR6′) had a negative correlation with the use of insulin (r = −0.24) and a positive correlation with the use of metformin (r = 0.29).

Because clinical factors were naturally correlated with each other, possible spurious correlation and suppressor variables were investigated by means of multiple regression analysis. The model that predicted BEE from body composition alone is shown in **Table 3** (model 1). Another model included selected variables by stepwise estimation (model 2). Insulin secretion (CPR6′; P = 0.015), use of insulin (P = 0.012) and pulse rate (P = 0.011) were significant determinants of BEE in addition to FFM (P < 0.001) and fat mass (P = 0.006). These additional factors explained another 3.9% of the variability of BEE, and the adjusted coefficient of determination was 83.4%. Standardized coefficients of FFM, fat mass, insulin secretion (CPR6′), use of insulin, and pulse rate in model 2 were 0.82, 0.19, −0.16, −0.15, and 0.15, respectively. Variance inflation factors of variables in model 2 were all <1.5. Other plausible determinants (ie, FPG, mean preprandial PG, A_{1c}, dietary energy, use of sulfonylurea, use of metformin, age, and sex) were not selected as significant contributors by stepwise estimation. The effect of insulin secretion (CPR6′) in BEE adjusted for FFM, fat mass, use of insulin, and pulse rate is illustrated in **Figure 1**.

DISCUSSION

In the current study, endogenous insulin secretion and exogenous insulin administered in treatment were both significant independent variables that predicted BEE in Japanese patients with type 2 diabetes under MNT and medications. In addition, both factors were negatively correlated with BEE. The current results suggested that the effect of insulin, regardless of the endogenous or exogenous source, had a significant negative impact on energy expenditure in patients with fair glycemic control under medical care.

In the current study, clinical factors regarding the effects of insulin predicted BEE, whereas factors regarding glycemic control did not predict BEE. The cause of these differing results is not clear, but the present results indicated that the effects of insulin affected BEE independently of glycemia. In a previous report, EGO was shown to be a significant predictor of elevated REE of patients with diabetes after adjustment for body composition, but the glucose concentration was not (18). Although FPG was correlated with EGO, it accounted for only 21% of its variability (19). Gluconeogenesis is an energy-consuming metabolic pathway and is thought to be a major source of increased EGO in diabetes (20–22). Because hepatic insulin deficiency plays an important role in increased gluconeogenesis in diabetes

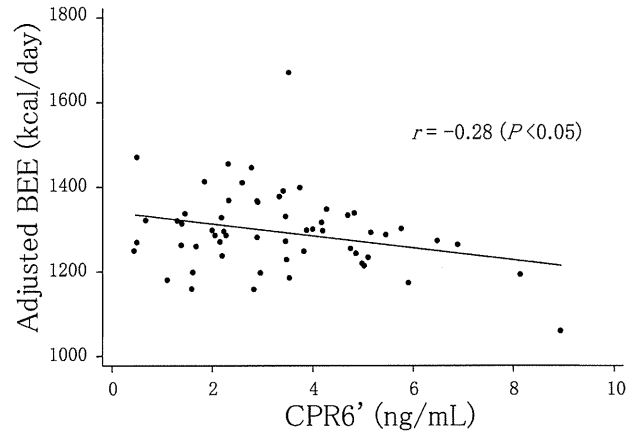

FIGURE 1. Relation between CPR6′ and BEE after adjustment for fat-free mass, fat mass, pulse rate, and insulin use (n = 58). BEE, basal energy expenditure; CPR6′, C-peptide immunoreactivity 6 min after intravenous glucagon injection.

(19), insulin, both endogenous and exogenous, may suppress BEE by reducing gluconeogenesis.

Protein turnover is also involved in energy expenditure. Protein turnover is often elevated in diabetes and has been shown to be correlated with REE in type 2 diabetes (23, 24). Because the treatment-induced reduction of nitrogen flux, which is an index of protein turnover, has been shown to be correlated with the C-peptide response to an oral glucose challenge (8), protein turnover may well play a role in the alteration of energy expenditure by insulin. In addition, impairment of insulin release is often accompanied by hyperglucagonemia in fasting and postprandial states in type 2 diabetes (25). Hyperglucagonemia is responsible for increased leucine oxidation and REE by insulin deprivation in type 1 diabetes (26). In addition, thermogenesis, especially via β-3 adrenergic receptors, has another impact on energy expenditure (20, 27). Considered together, these findings suggested that glucagon and catecholamine may also affect BEE in type 2 diabetes. However, we did not measure glucagon and catecholamine, which was a limitation of the current study.

Contrary to our results, the fasting insulin concentration has been reported to be positively correlated with energy expenditure (18). In the report (18), the positive correlation between insulin and energy expenditure was speculated to derive from the activation of the sympathetic nervous system by insulin (28). We showed that CPR6′ and insulin use were negatively correlated with BEE independently of the pulse rate, which is an indicator of the sympathetic nerve system activity, and was positively correlated with BEE independently of CPR6′ and insulin use. These findings suggested that the effect of insulin on BEE may be independent of the sympathetic nerve system activity at least in patients under treatment.

The difference in insulin sensitivity between lean Japanese subjects and obese American subjects may account for the difference in association of insulin with BEE. In general, a greater attribution of impaired insulin secretion and a lesser contribution of insulin resistance to glucose intolerance were shown in Japanese patients with type 2 diabetes, whose average BMI is ~25 but which is >30 in European and American populations (29). This difference may be attributable, in part, to the difference in BMI; in the Swedish population, the average CPR6′ is lower (~2 ng/mL) in lean subjects with BMI of ~25 than it is in obese subjects (~8 ng/mL) with BMI of ~30. Thus, our findings are in accord with those in Swedish lean subjects (30). Our previous finding of a positive correlation between BMI and CPR6′ also supported this attribution of difference in insulin secretion to difference in BMI (31).

Glycemia was shown to not be an independent determinant of BEE in this study. Although elevated BEE or REE after adjustment for body composition in patients with diabetes compared with in healthy subjects has been reported, the glucose concentration was not described (4, 5). Another study reported a significantly greater REE in patients with high glucose values (>10 mmol/L) compared with in patients with low glucose values (<10 mmol/L) (32). In addition, no increase in BEE was shown in patients with glycemic concentrations of ~9.5 mmol/L (6). Blood glucose concentrations of patients in the current study were improved by treatment, and FPG concentrations and mean preprandial PG concentrations were ~115 mg/dL (6.4 mmol/L) and 144 mg/dL (8.0 mmol/L) respectively. Therefore, the finding of no association between BEE and PG concentrations in the current study was not discrepant with previous reports and was in accord with the finding that REE did not significantly correlate with fasting glucose in type 2 diabetes in which the fasting glucose concentration was ~7.4 mmol/L (18). Together, these data suggested that glycemia is not an important factor in the prediction of BEE in patients with diabetes under treatment.

Dietary energy, treatment with sulfonylurea or metformin, age, and sex were not significant variables that predicted BEE. Sex itself was not a significant determinant but affected coefficients of FFM and fat mass when added to model 2. Researchers have noted a contribution of sex to BEE in addition to FFM and fat mass, although information of menstruation at the measurement of BEE was absent (4, 5). In the current study, BEE was measured during the follicular phase in accordance with a strict protocol for premenopausal women to avoid the influence of progesterone, which was supposed to increase energy expenditure. Another possibility is that our sample size was not large enough to show the contribution of sex to BEE. Last, with consideration of our previous finding that CPR6′ was independently influenced by BMI and the duration of diabetes in type 2 diabetes (31), we performed a regression analysis by adding these 2 putative covariates to model 2, which showed the insignificance of these determinants.

In conclusion, the current study shows that endogenous and exogenous insulin both have a significant impact on lowering BEE in patients with type 2 diabetes under standard treatment with MNT and medications. Longitudinal studies are required to elucidate the impact of the increment of C-peptide concentrations by insulinotropic agents and the administration of insulin on energy expenditure and gluconeogenesis during fair glycemic control.

We thank Tomoko Yokota for her assistance in conducting this research.

The authors' responsibilities were as follows—KI, SF, MG, and TK: designed the research; KI, CY, AH, and KS: conducted the research; KI, MG, and SF: analyzed data; KI and SF: wrote the manuscript; NI: supervised the research; SF: had primary responsibility for the final content of the manuscript; and all authors: read and approved the final manuscript. None of the authors had a conflict of interest.

REFERENCES

1. American Diabetes Association, Bantle JP, Wylie-Rosett J, Albright AL, Apovian CM, Clark NG, Franz MJ, Hoogwerf BJ, Lichtenstein AH, Mayer-Davis E, et al. Nutrition recommendations and interventions for diabetes: a position statement of the American Diabetes Association. Diabetes Care 2008;31(suppl 1):S61–78.
2. Cunningham JJ. Body composition as a determinant of energy expenditure: a synthetic review and a proposed general prediction equation. Am J Clin Nutr 1991;54:963–9.
3. Javed F, He Q, Davidson LE, Thornton JC, Albu J, Boxt L, Krasnow N, Elia M, Kang P, Heshka S, Gallagher D. Brain and high metabolic rate organ mass: contributions to resting energy expenditure beyond fat-free mass. Am J Clin Nutr 2010;91:907–12.
4. Bitz C, Toubro S, Larsen TM, Harder H, Rennie KL, Jebb SA, Astrup A. Increased 24-h energy expenditure in type 2 diabetes. Diabetes Care 2004;27:2416–21.
5. Martin K, Wallace P, Rust PF, Garvey WT. Estimation of resting energy expenditure considering effects of race and diabetes status. Diabetes Care 2004;27:1405–11.
6. Ryan M, Sallé A, Guilloteau G, Genaitay M, Livingstone MB, Ritz P. Resting energy expenditure is not increased in mildly hyperglycaemic obese diabetic patients. Br J Nutr 2006;96:945–8.
7. Nair KS, Halliday D, Garrow JS. Increased energy expenditure in poorly controlled Type 1 (insulin-dependent) diabetic patients. Diabetologia 1984;27:13–6.

8. Gougeon R, Pencharz PB, Sigal RJ. Effect of glycemic control on the kinetics of whole-body protein metabolism in obese subjects with non-insulin-dependent diabetes mellitus during iso-and hypoenergetic feeding. Am J Clin Nutr 1997;65:861–70.
9. Bursztein S, Elwyn DH, Askanazi J, Kinney JM. Energy metabolism, indirect calorimetry, and nutrition. Baltimore, MD: Lippincott Williams & Wilkins, 1989.
10. Compher C, Frankenfield D, Keim N, Roth-Yousey L; Evidence Analysis Working Group. Best practice methods to apply to measurement of resting metabolic rate in adults: a systematic review. J Am Diet Assoc 2006;106:881–903.
11. Frary CD, Johnson RK. Energy. In: Mahan LK, Escott-Stump S. Krause's food & nutrition therapy. 12th ed. St. Louis, MO: Saunders/Elsevier, 2007:22–38.
12. Japan Diabetes Society. Treatment guide for diabetes. Tokyo, Japan: Bunkodo, 2007.
13. Henry CJ. Basal metabolic rate studies in humans: measurement and development of new equations. Public Health Nutr 2005;8:1133–52.
14. Weir JB. New methods for calculating metabolic rate with special reference to protein metabolism. J Physiol 1949;109:1–9.
15. American Diabetes Association. Standards of medical care in diabetes-2011. Diabetes Care 2011;34(suppl 1):S11–61.
16. The Committee of the Japan Diabetes Society on the Diagnostic Criteria of Diabetes Mellitus. Report of the committee on the classification and diagnostic criteria of diabetes mellitus. J Diabetes Invest 2010;1: 212–28.
17. Faber OK, Binder C. C-peptide response to glucagon. A test for the residual beta-cell function in diabetes mellitus. Diabetes 1977;26:605–10.
18. Weyer C, Bogardus C, Pratley RE. Metabolic factors contributing to increased resting metabolic rate and decreased insulin-induced thermogenesis during the development of type 2 diabetes. Diabetes 1999; 48:1607–14.
19. Boden G, Chen X, Stein TP. Gluconeogenesis in moderately and severely hyperglycemic patients with type 2 diabetes mellitus. Am J Physiol Endocrinol Metab 2001;280:E23–30.
20. Nelson DL, Cox MM. Lehninger principles of biochemistry. 5th ed. New York, NY: WH Freeman and Company, 2008.
21. Consoli A, Nurjhan N, Capani F, Gerich J. Predominant role of gluconeogenesis in increased hepatic glucose production in NIDDM. Diabetes 1989;38:550–7.
22. Nuttall FQ, Ngo A, Gannon MC. Regulation of hepatic glucose production and the role of gluconeogenesis in humans: is the rate of gluconeogenesis constant? Diabetes Metab Res Rev 2008;24:438–58.
23. Stump CS, Nair KS. Alterations in protein metabolism in diabetes mellitus. 14th ed. In: Kahn CR, Weir GC, King GL, Jacobson AM, Moses AC, Smith RJ, eds. Joslin's diabetes mellitus. Boston, MA: Joslin diabetes center, 2005:275-90
24. Gougeon R, Morais JA, Chevalier S, Pereira S, Lamarche M, Marliss EB. Determinants of whole-body protein metabolism in subjects with and without type 2 diabetes. Diabetes Care 2008;31:128–33.
25. Dunning BE, Gerich JE. The role of α-cell dysregulation in fasting and postprandial hyperglycemia in type 2 diabetes and therapeutic implications. Endocr Rev 2007;28:253–8.
26. Charlton MR, Nair KS. Role of hyperglucagonemia in catabolism associated with type 1 diabetes. Diabetes 1998;47:1748–56.
27. Nonogaki K. New insights into sympathetic regulation of glucose and fat metabolism. Diabetologia 2000;43:533–49.
28. Anderson EA, Hoffman RP, Balon TW, Sinkey CA, Mark AL. Hyperinsulinemia produces both sympathetic neural activation and vasodilation in normal humans. J Clin Invest 1991;87:2246–52.
29. Fukushima M, Suzuki H, Seino Y. Insulin secretion capacity in the development from normal glucose tolerance to type 2 diabetes. Diabetes Res Clin Pract 2004;66:S37–43.
30. Dela F, von Linstow ME, Mikines KJ, Galbo H. Physical training may enhance β-cell function in type 2 diabetes. Am J Physiol Endocrinol Metab 2004;287:E1024.
31. Funakoshi S, Fujimoto S, Hamasaki A, Fujiwara H, Fujita Y, Ikeda K, Hamamoto Y, Hosokawa M, Seino Y, Inagaki N. Analysis of factors influencing pancreatic beta-cell function in Japanese patients with type 2 diabetes: association with body mass index and duration of diabetic exposure. Diabetes Res Clin Pract 2008;82:353–8.
32. Gougeon R, Lamarche M, Yale JF, Venuta T. The prediction of resting energy expenditure in type 2 diabetes mellitus is improved by factoring for glycemia. Int J Obes Relat Metab Disord 2002;26:1547–52.

Systems analysis of GLP-1 receptor signaling in pancreatic β-cells

Yukari Takeda, Akira Amano, Akinori Noma, Yasuhiko Nakamura, Shimpei Fujimoto and Nobuya Inagaki

Am J Physiol Cell Physiol 301:C792-C803, 2011. First published 6 July 2011;
doi:10.1152/ajpcell.00057.2011

Am J Physiol Cell Physiol 301: C792–C803, 2011.
First published July 6, 2011; doi:10.1152/ajpcell.00057.2011.

Systems analysis of GLP-1 receptor signaling in pancreatic β-cells

Yukari Takeda,[1] Akira Amano,[2] Akinori Noma,[2] Yasuhiko Nakamura,[1] Shimpei Fujimoto,[1] and Nobuya Inagaki[1]

[1]*Department of Diabetes and Clinical Nutrition, Graduate School of Medicine, Kyoto University, Kyoto; and* [2]*Faculty of Bioinformatics, Ritsumeikan University, Kusatsu City, Japan*

Submitted 3 March 2011; accepted in final form 28 June 2011

Takeda Y, Amano A, Noma A, Nakamura Y, Fujimoto S, Inagaki N. Systems analysis of GLP-1 receptor signaling in pancreatic β-cells. *Am J Physiol Cell Physiol* 301: C792–C803, 2011. First published July 6, 2011; doi:10.1152/ajpcell.00057.2011.—Glucagon-like peptide-1 (GLP-1) elevates intracellular concentration of cAMP ([cAMP]) and facilitates glucose-dependent insulin secretion in pancreatic β-cells. There has been much evidence to suggest that multiple key players such as the GLP-1 receptor, G_s protein, adenylate cyclase (AC), phosphodiesterase (PDE), and intracellular Ca^{2+} concentration ($[Ca^{2+}]$) are involved in the regulation of [cAMP]. However, because of complex interactions among these signaling factors, the kinetics of the reaction cascade as well as the activities of ACs and PDEs have not been determined in pancreatic β-cells. We have constructed a minimal mathematical model of GLP-1 receptor signal transduction based on experimental findings obtained mostly in β-cells and insulinoma cell lines. By fitting this theoretical reaction scheme to key experimental records of the GLP-1 response, the parameters determining individual reaction steps were estimated. The model reconstructed satisfactorily the dynamic changes in [cAMP] and predicted the activities of cAMP effectors, protein kinase A (PKA), and cAMP-regulated guanine nucleotide exchange factor [cAMP-GEF or exchange protein directly activated by cAMP (Epac)] during GLP-1 stimulation. The simulations also predicted the presence of two sequential desensitization steps of the GLP1 receptor that occur with fast and very slow reaction rates. The cross talk between glucose- and GLP-1-dependent signal cascades for cAMP synthesis was well reconstructed by integrating the direct regulation of AC and PDE by $[Ca^{2+}]$. To examine robustness of the signaling system in controlling [cAMP], magnitudes of AC and PDE activities were compared in the presence or absence of GLP-1 and/or the PDE inhibitor IBMX.[1]

adenylyl cyclase; glucagon-like peptide-1; model stimulation; phosphodiesterase

UPON ELEVATION of plasma glucose concentration ([glucose]), pancreatic β-cells generate bursts of action potentials to induce cyclic changes in $[Ca^{2+}]$ (55) and regulate pulsatile insulin release (25). This glucose-dependent insulin secretion is synergistically enhanced by incretin hormones, which are released upon meal ingestion from endocrine cells distributed over the intestinal tract (16). The incretin hormones include glucose-dependent insulinotropic peptide (GIP) and glucagon-like peptide-1 (GLP-1). GLP-1 is more effective than GIP to improve deteriorated incretin effect in diabetes and is widely used to treat patients with Type 2 diabetes (45). Elucidation of GLP-1 signaling system in β-cells, therefore, has been an extensive target of experimental studies. To date, it has been well established that GLP-1 activates adenylate cyclases (ACs) through binding to its G protein-coupled receptor and increases [cAMP], the key signal underlying the insulinotropic effects (17, 62).

The [cAMP] is determined primarily by the balance between cAMP production by ACs and degradation by phospodiesterases (PDEs) (8). The activities of several isoforms of AC and PDE expressed in β-cells are controlled by $[Ca^{2+}]$ (11, 28), which is regulated by Ca^{2+}-permeable ion channels and transporters as well as Ca^{2+} release and uptake by the endoplasmic reticulum (ER). The increase in [cAMP] subsequently activates protein kinase A (PKA) and exchange protein directly activated by cAMP (Epac), modulating the activities of multiple ion channels at the plasma membrane (26, 31, 35, 41, 42, 57) and ER (27, 36, 64), which in turn modify the pattern of Ca^{2+} transients. PKA and Epac also have direct effects on proteins that are involved in exocytosis of insulin vesicles (30), and thus the fine regulation of [cAMP] is critical for the adequate insulinotropic effects of GLP-1. However, since multiple signaling factors are involved in regulating [cAMP], the kinetic aspects of the reaction cascade during GLP-1 stimulation have not yet been determined in pancreatic β-cells.

To overcome this difficulty, we developed a mathematical model of GLP-1 receptor signal transduction. We adopted a strategy of estimating individual reaction rates and model parameters by fitting the theoretical reaction scheme to a variety of key experimental findings published to date (3, 11, 54, 66) in both β-cells and insulinoma cell lines. The model thus developed was validated by reconstructing the dynamic changes in [cAMP] during GLP-1 stimulation in the presence and absence of 3-isobutyl-1-methylxanthine (IBMX) observed under various experimental conditions. The model well-simulated GLP-1-induced [cAMP] elevation and predicted the activities of cAMP effectors PKA and Epac as a function of GLP-1. The simulation analysis revealed the presence of two transition steps of receptor desensitization that occur with fast and slow kinetics. The molecular basis for synergistic relationship between glucose and GLP-1 signaling in the cAMP synthesis were clarified by calculating the direct regulation of AC and PDE by $[Ca^{2+}]$. Finally, the robustness of the signaling system in controlling [cAMP] was examined by comparing the AC and PDE activities in the presence or absence of GLP-1 and/or the PDE inhibitor.

Glossary

[L]	GLP-1 (ligand)
[R]	free GLP-1receptor
$[R_t]$	total GLP-1 receptor
$[R_a]$	active GLP-1 receptor
$[R_{D1}]$	desensitized GLP-1 receptor in state 1
$[R_{D2}]$	desensitized GLP-1 receptor in state 2
[LR]	GLP-1 receptor bound with ligand

[1] This article is the topic of an Editorial Focus by Harvey (29a).

Address for reprint requests and other correspondence: N. Inagaki, 54 Shogoin, Kawahara-cho, Sakyo-ku, Kyoto-shi, Kyoto, Japan.

[LRG]	GLP-1 receptor bound with ligand and G_s
[G_t]	total G_s protein
[G]	G_s complex
[$G_{\beta\gamma}$]	β and γ subunit of G_s
[G_αGTP]	total GTP-bound α subunit of G_s
[G_αGDP]	GDP-bound α subunit of G_s
V_{AC_t}	total adenylate cyclase activity
V_C	activity of adenylate cyclase with G protein unbound
$V_{max\_AC\_t}$	Maximum activity of V_{AC}
V_{AC_G}	activity of adenylate cyclase with GαGTP
$V_{max\_AC\_G}$	maximum activity of V_{AC_G}
f_{Cd_AC}	fraction of Ca_xCaM-dependent V_{AC_G}
V_{Cd_AC}	Ca_xCaM-dependent component of V_{AC_G}
[CaM]	Calmodulin
[Ca_xCaM]	Calmodulin bound with Ca^{2+} ions ([Ca_3CaM]+[Ca_4CaM])
[Ca_3CaM]	Calmodulin bound with 3 Ca^{2+} ions
[Ca_4CaM]	Calmodulin bound with 4 Ca^{2+} ions
V_{PDE}	activity of phosphodiesterase
V_{max_PDE}	maximum activity of V_{PDE}
K_{mL}	low K_m of PDE
K_{mH}	high K_m of PDE
f	fraction of PDE with K_{mL}
f_{Cd_PDE}	fraction of Ca_xCaM-dependent V_{PDE}
V_{Cd_PDE}	Ca_xCaM-dependent component of V_{PDE}

METHODS

A minimal model of the GLP-1 receptor signaling transduction in pancreatic β-cells was constructed. Parameters to define the model, including concentrations, binding constants (K_d) of signaling factors, maximum activity (V_{max}) and half-maximal effective concentration ($K_{1/2}$) of substances for activation of enzymes, rate constants, and various magnitude factors of kinetic equations are listed in APPENDIX I. The time-based integration of six differential equations (*Eqs. 3–8*) were performed using the Euler method with a time step of <2 ms on the Microsoft Visual Studio platform. The units of time and substrate concentrations are secons and millimolar (indicated otherwise), respectively.

Activation of GLP-1 receptor. Figure 1 shows the reaction scheme of the minimal model of the GLP-1 receptor cascade. Active receptors may form three different conformations: free receptor (R), ligand (L)-bound receptor (LR), and the Gs-bound LR complex (LRG). Binding reactions indicated by black arrows were assumed to be much faster than the rest of reactions associated with conformational changes (22), and thus an instantaneous equilibrium was assumed for the reactions enclosed within the red rectangle. The dissociation constant (K_d) for GLP-1 binding to the receptor has been determined in expression systems (43, 65), whereas K_d for LR and G was estimated by fitting the [GLP-1]-dependent [cAMP] accumulation (66). In calculating the reaction cascade, total amounts [R_t] and [G_t] were conserved by applying *Eqs. 1* and *2*, respectively.

$$[R_t] = [R_a] + [R_{D1}] + [R_{D2}] \quad \text{Where } [R_a] = [R] + [LR] + [LRG]. \tag{1}$$

$$[G_t] = [G_{\alpha\beta\gamma}] + [G_{\beta\gamma}] \quad \text{Where } [G_{\alpha\beta\gamma}] = [G] + [LRG] \tag{2}$$

Upon ligand binding, the GLP-1 receptor undergoes desensitization through phosphorylation by unknown mechanisms (67). Although the molecular mechanism has not been elucidated, the computer simulation of the spontaneous decay in [cAMP] during continuous stimulation with GLP-1 (see Fig. 3) as well as desensitized [cAMP] production after preconditioning of GLP-1 receptors (see Fig. 4) suggested the presence of two sequential desensitization states R_{D1} and R_{D2}. We assume that the first desensitization step to R_{D1} occurs from the ligand-bound form of the receptor, (LR + LRG), followed by the second transition to R_{D2} with a recovery steps to R_a (see Fig. 1). The rate constants for the time-dependent desensitization were determined by fitting the kinetic sheme to experimental recordings, and the time-dependent changes in [R_{D1}] and [R_{D2}] are defined with *Eqs. 3* and *4*, respectively.

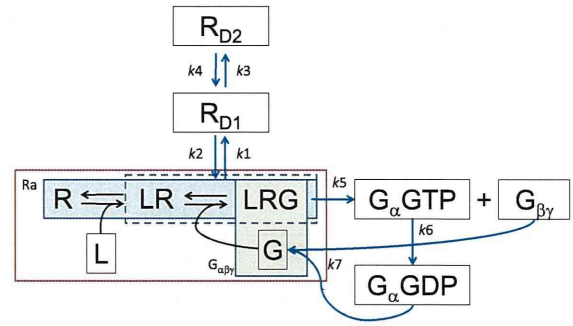

Fig. 1. Reaction scheme of glucagon-like peptide-1 (GLP-1) receptor activation. The receptor takes five different conformations: R, free receptor; LR, ligand (L)-bound form; LRG, G_s-bound LR complex; R_{D1}, desensitized receptor at the state D1 with faster kinetics defined by rate constants *k1* and *k2*; and R_{D2}, desensitized receptor at the state D2 with the very slow kinetics defined by rate constants *k3* and *k4*. The desensitization to R_{D1} occurs only from the ligand bound form (LR and LRG) with *k1*, and the recovery to active receptos (R_a) (= R + LR + LRG) with *k2*. States of G_s protein include $G_{\alpha\beta\gamma}$, heterotrimeric complex (for [G] and [LRG]) and dissociated subunits G_αGTP, G_αGDP, and $G_{\beta\gamma}$. Time-dependent changes in conformations of G protein are calculated by rate constants of G_s dissociation into G_αGTP and $G_{\beta\gamma}$ subunits (*k5*), subsequent hydrolysis of GTP (*k6*), and reassociation of G_αGDP with $G_{\beta\gamma}$ (*k7*). The reaction steps marked with a black arrow were calculated assuming instantaneous equilibrium, whereas those marked with blue arrows were calculated by the time-based integration using the Euler method. When calculating the instantaneous equilibrium enclosed with the red rectangle, the constraint of mass conservation was applied to the sum of (R + LR + LRG) and (G + LRG), respectively, at each time step.

$$d[R_{D1}]/dt = k1 \cdot ([LR] + [LRG]) - k2 \cdot [R_{D1}] - k3 \cdot [R_{D1}] + k4 \cdot [R_{D2}] \tag{3}$$

$$d[R_{D2}]/dt = k3 \cdot [R_{D1}] - k4 \cdot [R_{D2}] \tag{4}$$

The kinetics for the activation and deactivation of G protein are calculated by rate constants of G dissociation into G_αGTP and $G_{\beta\gamma}$ subunits and subsequent hydrolysis of GTP (APPENDIX I), which have been biochemically investigated (5, 56). The time-dependent changes in [G_αGTP], [G_αGDP], and [$G_{\beta\gamma}$] are described by the following differential equations:

$$d[G_\alpha GTP]/dt = k5 \cdot [LRG] - k6 \cdot [G_\alpha GTP] \tag{5}$$

$$d[G_\alpha GDP]/dt = k6 \cdot [G_\alpha GTP] - k7 \cdot [G_\alpha GDP] \cdot [G_{\beta\gamma}] \tag{6}$$

$$d[G_{\beta\gamma}]/dt = k5 \cdot [LRG] - k7 \cdot [G_\alpha GDP] \cdot [G_{\beta\gamma}] \tag{7}$$

AC and PDE activities. The level of [cAMP] is determined by the balance between production rate (V_{AC_t}) and degradation rate (V_{PDE}) by ACs and PDEs, respectively (*Eq. 8*).

$$\frac{d[cAMP]}{dt} = V_{AC\_t} - V_{PDE} \tag{8}$$

At least nine different isoforms of membrane-bound AC have been identified (29). In pancreatic β-cells, ACVIII was suggested to play a predominant role in synthesis of cAMP during GLP-1 stimulation of β-cells (53). The modulation of ACVIII by both Ca^{2+}-bound calmodulin (Ca_xCaM) and $G_{s\alpha}$GTP would provide the molecular basis for synergistic relationship between glucose and GLP-1 stimulation in the cAMP synthesis (11). In addition to this adaptable component

(V_{AC_G}), a basal component (V_{AC}) was assumed to maintain the resting [cAMP] in the absence of agonists. Thus the total activity of ACs (V_{AC_t}) is given by a sum of V_{AC} and V_{AC_G} (*Eqs. 9–11*).

$$V_{AC\_t} = V_{AC} + V_{AC\_G} \quad (9)$$

$$V_{AC} = V_{max\_AC} \cdot \frac{0.0004}{0.0004 + G_\alpha GTP} \cdot \frac{[ATP]}{[ATP] + 1.03} \quad (10)$$

$$V_{AC\_G} = V_{max\_AC\_G} \cdot \frac{G_\alpha GTP}{0.0004 + G_\alpha GTP} \cdot \frac{[ATP]}{[ATP] + 0.315} \times \left((1 - f_{Cd\_AC}) + f_{Cd\_AC} \cdot \frac{[Ca_3CaM] + [Ca_4CaM]}{[Ca_3CaM] + [Ca_4CaM] + 0.000348} \times \frac{0.075}{0.075 + [Ca^{2+}]} \right) \quad (11)$$

The $G_\alpha GTP$-dependent activation of AC was calculated with a $K_{1/2}$ determined by Sunahara and colleagues (58). An [ATP] of 3 mM was used in the present study, and the $K_{1/2}$ of [ATP] defining the substrate dependency of V_{AC} and V_{AC_G} were adopted from Dessauer et al. (13). The term for Ca^{2+}-dependent regulation of V_{AC_G} in *Eq. 11* was originally developed in *Aplysia* neurons (69) and was modified to fit the ACVIII activity (21) in the β-cell model by Fridlyand et al. (23). *Eq. 11* contains both Ca_xCaM ([Ca_3CaM]+[Ca_4CaM])-mediated activation and Ca^{2+}-dependent inhibition. We additionally introduced f_{Cd_AC}, the fraction of Ca_xCaM-dependent V_{AC_G}. A [Ca^{2+}] of 500 nM was assumed under a high-glucose condition and a resting [Ca^{2+}] of 100 nM for a lower glucose concentration used in experiments (18, 33, 60). An instantaneous equilibrium was assumed for the binding of Ca^{2+} to CaM using the association and dissociation rate constants given by Yu and colleagues (69). The V_{AC_t} was determined at 1.8 μM/s from the initial rate of rise (dashed line in Fig. 3*A*) of [cAMP] evoked by GLP-1 in the presence of high [IBMX] > 250 μM and [glucose] > 20 mM. Based on this estimation, V_{max} of AC activities (V_{max_AC} and $V_{max\_AC\_G}$) and fractions (f) of the Ca^{2+}-dependent component of V_{AC_G}(f_{Cd_AC}) were optimized (see APPENDIX I) by reconstructing experimental findings with the whole reaction scheme.

In β-cells, it has been suggested that several PDE isoforms (1C, 3B, 4, 8B, and 10A) are involved in regulation of insulin secretion (15, 51). However, the fractional contribution of each isoform to cAMP degradation in intact cells has not yet been determined. Sams and Montague (54) observed over 70% of total PDE activity in the supernatant fraction of an homogenate of islets of Langerhans. Their kinetic analysis of the soluble PDEs suggested the presence of at least two fractions with different activities, as indicated by two linear components (dashed and solid black lines) in the Lineweaver-Burk plot (Fig. 2). We reevaluated the experimental results by fitting the data with a sum of two Michaelis-Menten functions (*Eq. 12*) in the present study.

$$V_{PDE} = V_{max\_PDE} \cdot \left(\frac{f \cdot [cAMP]}{[cAMP] + K_{mL}} + \frac{(1 - f) \cdot [cAMP]}{[cAMP_f] + K_{mH}} \right) \quad (12)$$

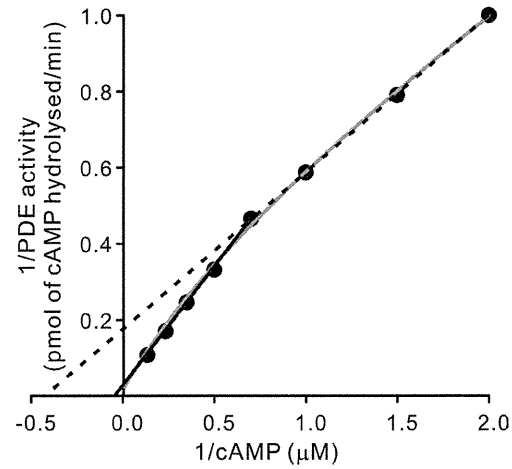

Fig. 2. Determination of K_m values of phosphodiesterase (PDE) based on experimental Lineweaver-Burk plots. Filled circles and fitted (dotted and black) lines are reproduction of experimental data (54) determined in guinea pig islets. The properties of the PDE activity components were reevaluated by fitting the experimental results with *Eq. 12* (solid gray line).

The fitting (gray curve in Fig. 2) determined the K_m values (K_{mL} and K_{mH}) and f of the two components. V_{PDE} thus reflects the sum of all PDE activities.

Since Ca_xCaM-sensitive PDE1C plays a functional role in degradation of cAMP in the β-cell lines βTC3 (28) and MIN6 (38), a Ca^{2+}-dependent component was added to the PDE model (*Eq. 13*).

$$V_{PDE} = V_{max\_PDE} \cdot \left(\frac{f \cdot [cAMP]}{[cAMP] + K_{mL}} + \frac{(1 - f) \cdot [cAMP]}{[cAMP] + K_{mH}} \right) \left[(1 - f_{Cd\_PDE}) + f_{Cd\_PDE} \cdot \frac{[Ca_3CaM] + [Ca_4CaM]}{[Ca_3CaM] + [Ca_4CaM] + 0.000348} \right] \quad (13)$$

The half-maximal value of Ca_xCaM for the stimulation of PDE (68) was adopted from the PDE model developed for β-cells (23), and f_{Cd_PDE} reflects the fraction of the Ca_xCaM-dependent component of the enzyme. Given the [cAMP]s determined under various experimental conditions (Table 1), V_{max_PDE} and f_{Cd_PDE} (APPENDIX I) were finely adjusted by reconstructing these experimental findings using 100 or 500 nM [Ca^{2+}] according to the [glucose] used in experiments.

In experimental studies, the rise in [cAMP] evoked by GLP-1 saturates even in the presence of a maximal inhibitory concentration of IBMX, indicating that some fraction of PDE activity still remained, controlling [cAMP]. Ahmad and colleagues (1) showed that ~80% of the soluble PDE activity in a β-cell line (BRIN-BD11 cells) was blocked by [IBMX] > 200 μM, and thus we assumed that the

Table 1. *Comparison of [cAMP] between experimental measurements in rat primary pancreatic β-cells and model simulations under control conditions and after 15 min stimulation with GLP-1 with or without IBMX*

	Experimental Data	Simulation Result	Experimental Data	Simulation Result
Experimental conditions:	1.4 mM Glucose	100 nM Ca^{2+}	20 mM Glucose	500 nM Ca^{2+}
cAMP levels, μM				
Resting (control)	3.4	1.6	3.2	1.4
10 nM GLP-1		4.2		5.6
Resting w/ IBMX	10.5	12.0	11.7	10.3
10 nM GLP-1w/ IBMX	38.2	37.0	55.2	57.6

The cAMP levels were indicated in units of fmol·10^3 $cells^{-1}$ in the experimental work (11), and we converted these units to μM by assuming the cytoplasmic volume of a single β-cell [764 fL; (10)]. Administration of IBMX (250 μM) was simulated by decreasing PDE activity by 80%. See text for definitions of abbreviations.

IBMX-insensitive PDE8 may contribute 20% PDE activity in the presence of a high [IBMX].

PKA and Epac activities. Although pancreatic β-cells most likely express both PKA type I and II (2, 37, 39), the isoform predominantly regulating the insulinotropic effect of GLP-1 has not been investigated. Since K_d of PKA type I [2.9 μM (9)] and the half-maximal [cAMP] for the activation of type II [$K_{1/2}$ = 2~3 μM (7)] were very similar, we included one hypothetical type of PKA in the present model, and the activity was calculated with a K_d of 2.9 μM (Hill coefficient, n_H = 1.4) determined by Dao et al. (9). Distinct values of $K_{1/2}$ were reported for Epac1 and 2 [30 μM for Epac1 (20) and 20 μM for Epac2 (52, 63)], and thus the active fractions were separately determined.

RESULTS

[cAMP] in pancreatic β-cells under resting conditions and GLP-1 stimulation. The basal level of [cAMP] was 1.6 μM at 100 nM [Ca^{2+}] and 1.4 μM at 500 nM [Ca^{2+}] in our model simulation (Table 1). These values of [cAMP] are comparable to 3.4 and 3.2 μM measured in rat primary β-cells at 1.4 and 20 mM [glucose], respectively (11). Upon stimulation with 10 nM GLP-1 for 15 min, [cAMP] increased to 4.2 μM at 100 nM [Ca^{2+}] and to 5.6 μM at 500 nM [Ca^{2+}] in our model. If PDE was inhibited by 80% (corresponding to 250 μM IBMX) in the absence of GLP-1, [cAMP] increased to ~11 μM independently of [Ca^{2+}] levels. These results also agreed well with the experimental observations. When stimulated with 10 nM GLP-1 in the presence of IBMX, [cAMP] elevated to 37.0 μM at 100 nM [Ca^{2+}] and further to 57.6 μM at 500 nM [Ca^{2+}], similarly to the experimental records of 38.2 and 55.2 μM obtained at the low (1.4 mM) and high (20 mM) [glucose], respectively.

The experimental time course of [cAMP] accumulation induced by GLP-1 (66) was also examined (Fig. 3). Upon stimulation with GLP-1 at 25 mM [glucose] in the presence of IBMX, [cAMP] increased rapidly and slowly declined after reaching peaks within 4 min (filled circles, Fig. 3*A*). The time course of [cAMP] was well reconstructed by simulation at 20% PDE activity and 500 nM [Ca^{2+}] (black curve, Fig. 3*A*). The velocity of cAMP degradation by PDE gradually increases with increasing [cAMP], and the peak is attained when the production rate of cAMP (V_{AC_t}) matched the degradation rate by PDE (V_{PDE} in *Eq. 8*). Simulations revealed that the time to peak as well as the subsequent slow decline in [cAMP] were also influenced by desensitization of the GLP-1 receptor, predominantly due to the state transition to R_{D1} (Fig. 1). In the absence of IBMX, the balance between AC and PDE activities are attained at a much lower [cAMP], thereby giving a time to peak of <1 min (gray curve, Fig. 3*A*). The simulation result was also in good agreement with experimental data (open circles, Fig. 3*A*).

The experimental dose-response relationship obtained by Widmann and colleagues (66) was reconstructed by calculating the [cAMP] accumulation attained over 10 min application of different concentrations of GLP-1 at 20% PDE activity and 500 nM [Ca^{2+}] (Fig. 3, *B* and *C*). At 0.001 and 0.01 nM [GLP-1], [cAMP] increased to a stable saturation level within 2 min (Fig. 3*B*), whereas at higher [GLP-1], the time to peak was delayed with increasing [GLP-1] and the desensitization became more pronounced. As [GLP-1] increases, the activation of V_{AC_G} (see *Eqs. 9~11*) became significant when [GLP-1] > 0.1 nM and nearly saturated at [GLP-1] slightly larger than 10 nM. In Fig. 3*C*, the dose-dependent accumulation of cAMP at the end of 10 min application of different concentrations of GLP-1 are compared between the simulation and experimental

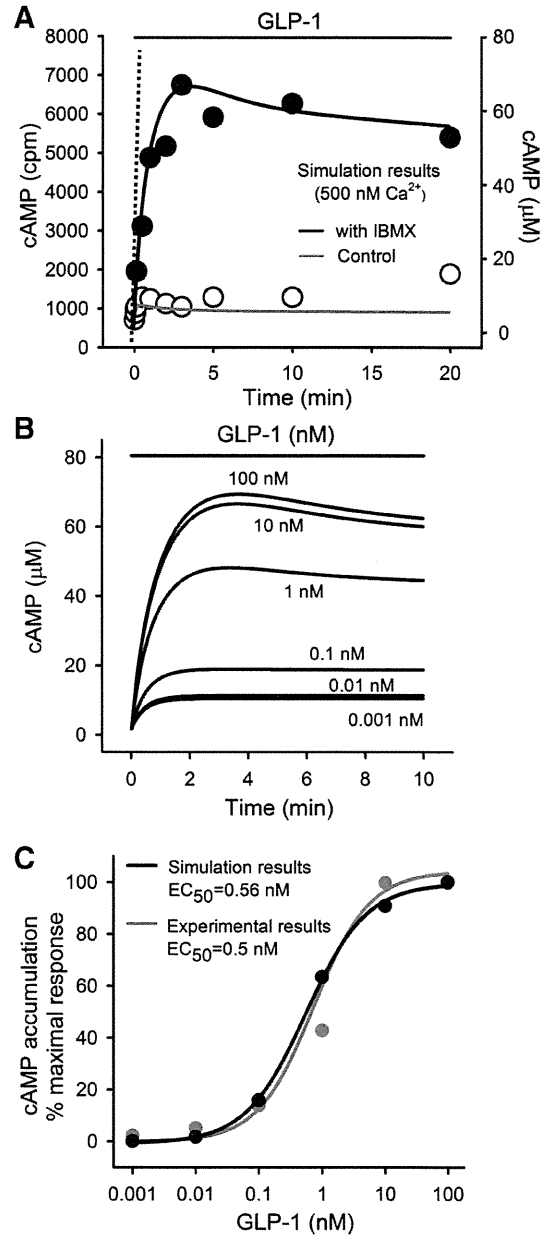

Fig. 3. Time courses of [cAMP] change induced by applying 100 nM GLP-1 (indicated by a horizontal line at the top). *A*: open circles (control) and filled circles [with 1 mM 3-isobutyl-1-methylxanthine (IBMX)] are reproduction of experimental data (66) obtained at 25 mM [glucose] in INS-1 cells. For conversion of units on the left to right vertical axes, see the legend of Table 1. The black and gray curves are simulation results at 500 nM [Ca^{2+}] with and without IBMX, respectively. A 20% activity of PDE was assumed in the presence of IBMX. The dotted line was fitted to the initial rate of rise of [cAMP] to determine the activity of adenylate cyclase (AC). *B*: simulated time courses of the dose-dependent [cAMP] accumulation at 500 nM [Ca^{2+}] during continuous GLP-1 stimulation under the presumptive presence of IBMX (PDE activity inhibited by 80%). *C*: [cAMP] responses to 10 min stimulation with GLP-1 expressed as the percentage of the maximal response in simulation (black line). The dose-response curve was compared with that measured in INS-1 cells (grey line) (66).

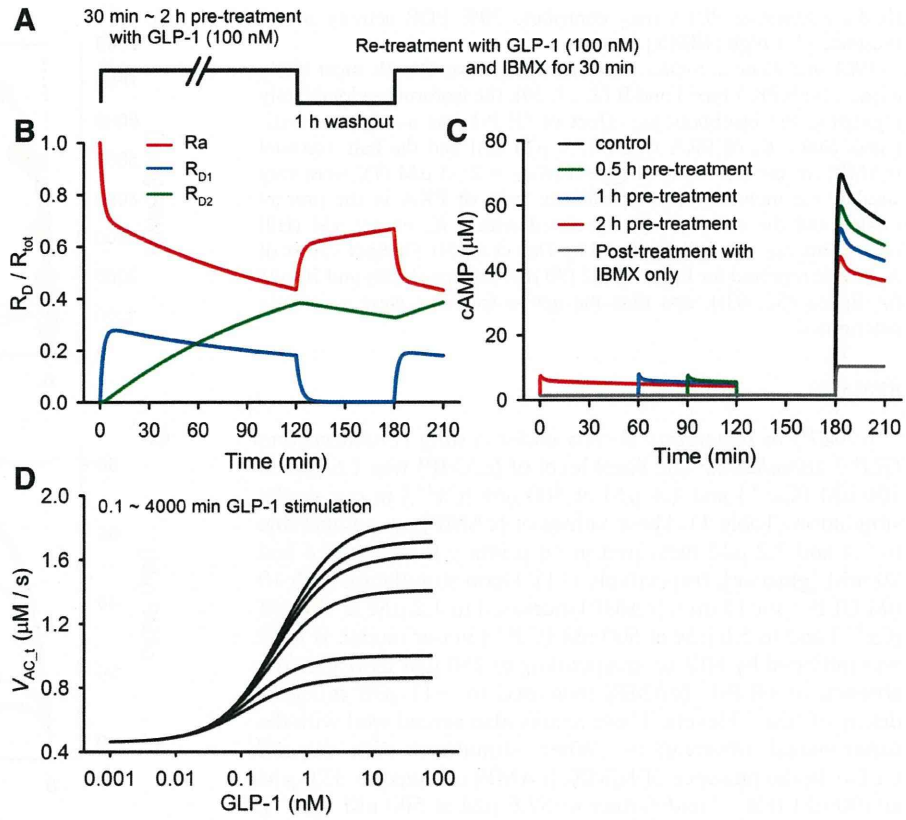

Fig. 4. GLP-1 receptor desensitization. *A*: protocol used in the experimental study of receptor desensitization (3). GLP-1 at 100 nM was applied for various conditioning periods of 30 min to 2 h followed by a 1-h pause before the test application of the same dose. IBMX was only applied with the second application of GLP-1. *B*: time course of the probability of R_a (red) and those of R_{D1} (blue) and R_{D2} (green) in response to the 2-h pretreatment protocol. *C*: [cAMP] response (at 500 nM [Ca^{2+}]) to the experimental protocol with varying pretreatment periods, indicated by different colors. The gray trace was obtained by applying IBMX only at the time point of 180 min. *D*: [GLP-1] − V_{AC_t} relations at the end of different stimulation periods of 6 s, 10 s, and 1, 2, 20, 200, 2,000, and 4,000 min, from *top* to *bottom* of 8 curves, respectively. The traces of 6 and 10 s stimulation almost overlapped with one another, indicating that the desensitization was invisible with these short periods, whereas traces with 2,000 and 4,000 min stimulation also overlapped, indicating saturation of the desensitization already at ~2,000 min.

results in INS-1 cells. The half-maximal [GLP-1] is 0.56 nM in the simulation, which is only slightly larger than that obtained in INS-1 cells (0.50 nM).

Ultra-slow desensitization of the GLP-1 receptor. The simulation analysis suggested that the gradual decay of [cAMP] after the peak (Fig. 3, *A* and *B*) during GLP-1 stimulation largely reflects desensitization of the ligand-bound receptor (LR and LRG in Fig. 1) to R_{D1}. However, the R_{D1} kinetics alone failed to reconstruct the very slow inactivation remaining 1 h after washing out agonist as observed by Baggio and colleagues (3). The model including an R_{D2} state in series with R_{D1} reconstructed well the desensitization phenomenon in response to the experimental protocol (Fig. 4*A*). When the 2-h prestimulation protocol was applied (Fig. 4*B*), the R_{D1} fraction (blue curve) increased to a maximum of ~0.28 at the expense of the active fraction (R_a, red curve) within the initial 10 min, and then both R_a and R_{D1} slowly declined thereafter due to a continuous transition to R_{D2} (green curve). During the washout period, the R_{D1} fraction quickly became insignificant, whereas 85% of R_{D2} remained even after 1 h washout. The result suggests that the fraction of R_a available for the second application of GLP-1 decreases depending on the preincubation period. Figure 4*C* shows the [cAMP] response to the experimental protocol with varying pretreatment periods. It is evident, as predicted, that the longer the preincubation period, the more the [cAMP] response was reduced on the second application of GLP-1. The reductions (in %) in [cAMP] accumulations on the second stimulus were normalized to the control amplitude and were summarized in Table 2. These results agreed well with the experimental observations (3).

To characterize the steady-state desensitization of the GLP-1 receptor, the [GLP-1]-dependent V_{AC_t} at varying incubation periods (10 s ~ 4,000 min) were computed over the range 0.001~100 nM [GLP-1] (Fig. 4*D*). With 6- and 10-s applications, V_{AC_t} nearly overlap one another virtually without any sign of receptor desensitization. When the duration of GLP-1 application was prolonged, the desensitization gradually developed and a steady state was obtained at ~2,000 min application, which gave ~25% of the control V_{AC_t} at the saturating [GLP-1]. The extent of desensitization was more pronounced when stimulated with higher [GLP-1].

Cross-talk between glucose and GLP-1 signal pathways in determining [cAMP]. Experimental studies in Min6 and INS-1 β-cells demonstrated that [cAMP] increased in phase with a temporal increase in [Ca^{2+}] in the presence of GLP-1, whereas

Table 2. *Reduction of GLP-1-dependent [cAMP] accumulation induced by prestimulation of receptors for different time periods*

	Preincubation Period With 100 nM GLP-1		
	0.5 h	1 h	2 h
% Reduction			
Simulation results	16	26	40
Experimental results	21	35	50

The [cAMP] accumulation caused by IBMX alone (Fig. 4*C*) was subtracted from the [cAMP] responses to the second application of agonist, and the differences were normalized to the control value. The simulation results are compared with the experimental data in INS-1 cells (3). See text for definitions of abbreviations.

the relation between [cAMP] and [Ca^{2+}] was out of phase without agonist (19, 23, 38). The simulation in Fig. 5 examines mechanisms of [Ca^{2+}]-dependent regulation of [cAMP] in the absence or presence of GLP-1. In the absence of GLP-1, the total cAMP production rates V_{AC_t} (V_{AC} + V_{AC_G}) matched the V_{PDE} at a resting [cAMP] of 1.6 μM (black curve in Fig. 5*A*) at 100 nM [Ca^{2+}]. When [Ca^{2+}] was increased to 500 nM (grey curve), [cAMP] slightly decreased to 1.4 μM due to the facilitation of PDE activity by [Ca^{2+}] (V_{Cd_PDE}, grey curve in Fig. 5*C*). After 30 min simulation with 100 nM [GLP-1], [cAMP] increased to 4.1 μM (Fig. 5*B*) due to enhanced V_{AC_G} at 100 nM [Ca^{2+}]. Increasing [Ca^{2+}] to 500 nM further elevated [cAMP] in a reversible manner up to 5.4 μM because the activation of AC_G by [Ca^{2+}] (V_{Cd_AC}, black curve in Fig. 5*D*) was relatively larger than that of PDE (V_{Cd_PDE}). These simulation results revealed the mechanisms underlying the in-phase or out-of-phase patterns of [cAMP] fluctuations in response to the cyclic changes in [Ca^{2+}] (19, 23, 38). To get a deeper insight into the physiological significance of [Ca^{2+}] in determining [cAMP], the changes in [cAMP] in response to increasing [Ca^{2+}] from 0.05 to 5.0 μM were simulated at varying [GLP-1]. The depression of [cAMP] response induced by increasing [Ca^{2+}] at a lower [GLP-1] was inverted at ~0.054 nM [GLP-1], and the enhancement of [cAMP] synthesis by [Ca^{2+}] was augmented further with increasing [GLP-1], saturating at ~2 μM [Ca^{2+}] (Fig. 5*E*). Note that with higher [Ca^{2+}] (≳5 μM), cAMP response to GLP-1 starts to decrease, reflecting the [Ca^{2+}]-dependent inactivation (see *Eq. 11*).

Activation of PKA and Epac by GLP-1. Time courses of [cAMP] responses to GLP-1 were measured using a PKA-based biosensor in INS-1 cells (19). The fluorescent signals were detected using evanescent wave microscopy reflecting [cAMP] in the submembrane space. However, since the signals were not calibrated, extent of PKA activation by the GLP-1 stimulus was not obtained from the experimental results. We thus attempted to predict PKA activity using the GLP-1 receptor signal cascade model developed in the present study (Fig. 6). Toward this end, it was essential to examine the localization of cAMP under the surface membrane compared with the bulk [cAMP], since the PKA activities may vary within the cytosol due to an uneven distribution of cAMP. In pancreatic β-cells, highly localized cAMP microdomain may possibly be present

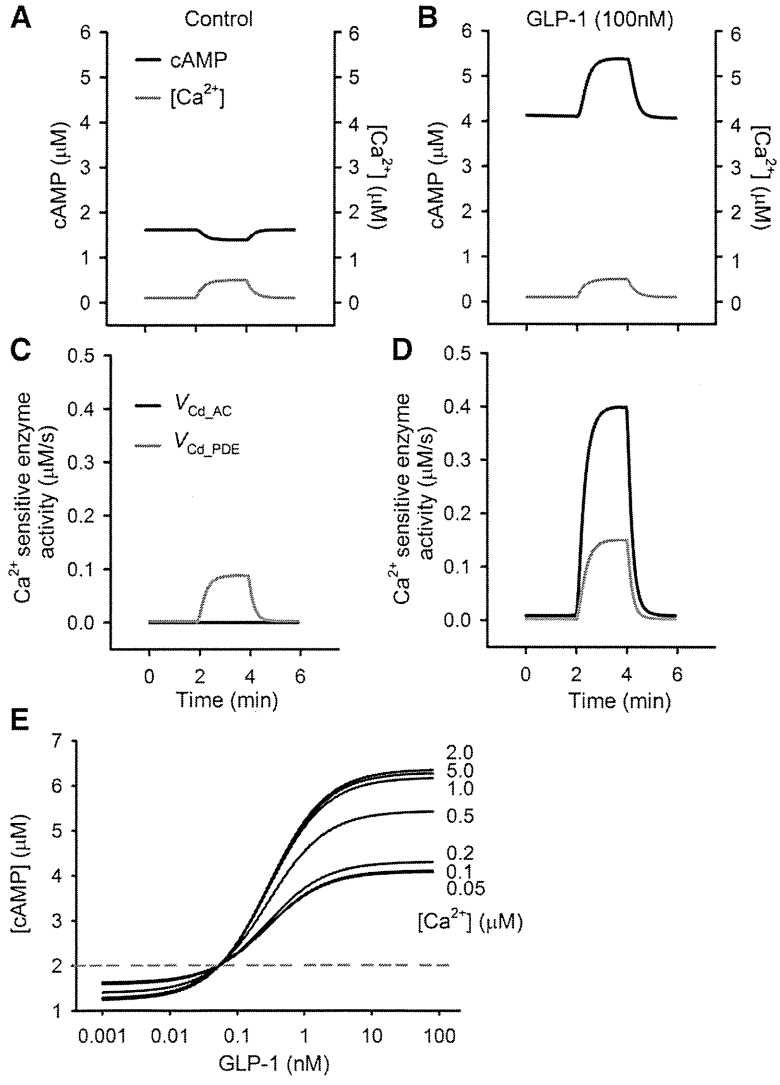

Fig. 5. [cAMP] responses to changes in [Ca^{2+}]. *A* and *B*: [Ca^{2+}] (gray lines) was varied from 100 to 500 nM with a time constant of 30 s in the absence (*A*) or presence (*B*) of 100 nM GLP-1. [cAMP] (black lines) responses to the corresponding [Ca^{2+}]. *C* and *D*: [Ca^{2+}]-dependent AC_G (V_{Cd_AC}, black line) and PDE (V_{Cd_PDE}, grey line) activities under the conditions examined in *A* and *B*, respectively. *E*: [GLP-1]-[cAMP] response curves at varying [Ca^{2+}] (0.05, 0.1, 0.2, 0.5, 1.0, 2.0, and 5.0 μM). Dotted gray line indicates [cAMP] at [GLP-1] = 0.054 nM, where decreasing [cAMP] responses to increasing [Ca^{2+}] at a lower [GLP-1] is converted to increasing [cAMP].

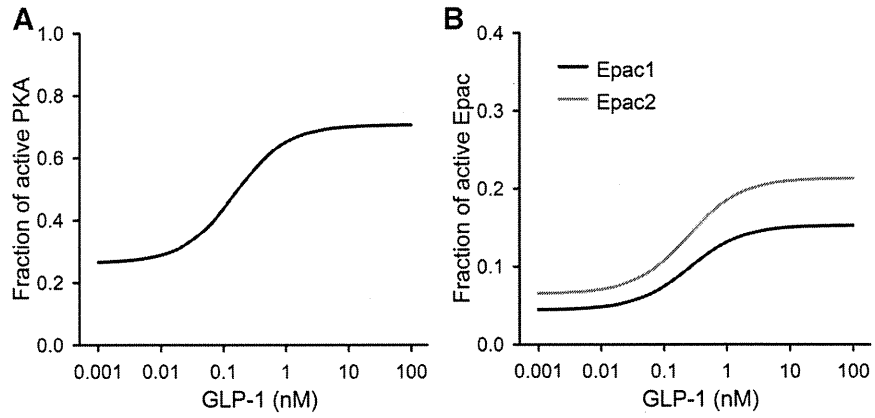

Fig. 6. Dose-dependent activities of protein kinase A (PKA) and exchange protein directly activated by cAMP (Epac) at 500 nM [Ca^{2+}] after 30 min stimulation with various concentrations of GLP-1. *A*: fraction of active PKA. *B*: fractions of active Epac1 (black line) and 2 (grey line).

at submembrane space, since production of cAMP by ACs is limited at the surface membrane (29, 38), while PDE-mediated degradation occurs diffusely within the cytosol (4, 54). Indeed, cAMP microdomain has been observed beneath the surface membrane in other cell types, such as cardiac myocytes (70) and HEK cells (61).

To simulate the distribution of [cAMP], intracellular diffusion of cAMP was calculated (Fig. 7). For simplicity, one-dimensional diffusion was assumed over a distance of 4 μm (estimated from Ref. 48) from the surface membrane toward the nucleus as indicated in Fig. 7*A*. The diffusion path (x) was separated into 200 compartments, and [cAMP] in each compartment at time t [C (x,t)] was calculated using the following equation:

$$\frac{\partial C(x,t)}{\partial t} = D \cdot \frac{\partial^2 C(x,t)}{\partial x^2} \qquad (14)$$

With boundary condition of

$$\left.\frac{\partial C}{\partial x}\right|_{x=0,4} = 0$$

where the diffusion coefficient (D) was 0.3 μm^2/ms based on experimental measurements of 0.27 μm^2/ms (6) and 0.33 μm^2/ms (32). The cAMP production by AC stimulated by a [GLP-1] of 10 nM was assumed only in the first compartment (29, 38), whereas cAMP degradation by PDE was calculated in all compartments (4, 54). A quasi-steady-state concentration gradient of [cAMP] was established within 100 ms after the onset of AC activation, and the difference in [cAMP] over the diffusion path of 4 μm was only about 0.05 μM. Theoretically, but unrealistically, a much larger gradient (4 μM) was developed only when V_{PDE} was increased by 100 times. The distributions of [cAMP] relative to [cAMP] in the submembrane space simulated using the control and high V_{PDE} are shown in Fig. 7, *B* and *C*, respectively. This finding agrees with simulation results demonstrated by Oliveira et al. (47) (see DISCUSSION for more detail). The flat distribution in Fig. 7*B* may justify the use of average [cAMP] in estimation of active fractions of cAMP effecters that are distributed throughout the cytosol of pancreatic β-cells.

With the use of the GLP-1 receptor signal transduction model, the dose-dependent activities of PKA at the end of 30 min application of various concentrations (0.001~100 nM) of GLP-1 under high [Ca^{2+}] condition were simulated (Fig. 6*A*). The [cAMP]-dependent PKA activation was calculated using a

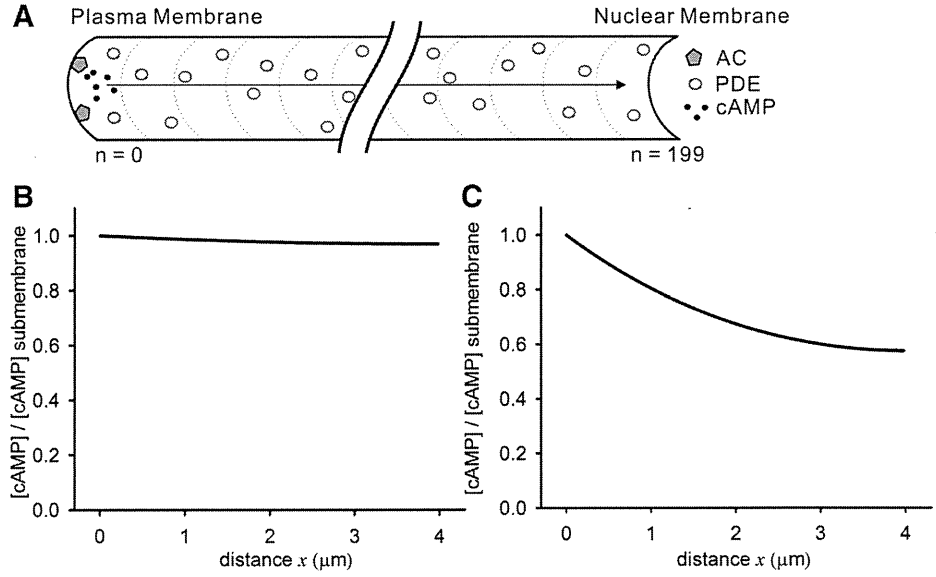

Fig. 7. [cAMP] gradient in the cytosol of a pancreatic β-cell during GLP-1 stimulation. *A*: one-dimensional diffusion of cAMP (arrow) was assumed from the surface membrane (*left*) toward the nuclear membrane (*right*) over a distance of 4 μm. The diffusion path was separated into 200 compartments, and AC activity was included only in the first compartment, while a homogeneous PDE distribution was assumed in all compartments. V_{AC} and V_{PDE} under 10 nM GLP-1 stimulation at 500 nM [Ca^{2+}] were applied for the calculation. *B*: gradient of [cAMP] over the distance of diffusion path in a pancreatic β-cell. *C*: [cAMP] gradient obtained with the same experimental conditions as in *B* except V_{max_PDE} was multiplied by 100.

K_d and nH (see APPENDIX I) obtained by Dao et al. (9). A significant fraction (~26%) of PKA was already active under the control condition of 1.4 μM [cAMP] at 500 nM [Ca^{2+}] without GLP-1 stimulation. As shown in Fig. 6*A*, the activity of the enzyme dose dependently increased, and the application of 100 nM [GLP-1] induced nearly the saturating activation of PKA (~70%) through an increase in [cAMP] to 5.4 μM. With the same experimental conditions as in Fig. 6*A*, the active fractions of Epac1 and 2, other cAMP effectors, were also simulated using the half-maximal values of cAMP for the activation of each enzyme (APPENDIX I). GLP-1 at 100 nM activates Epac1 from 4.4% of basal activity to 15.3%, whereas active Epac2 was about 6.4% at rest and was increased to ~21.3% (Fig. 6*B*).

Systems analysis on the balance between the production and degradation of cAMP. The level of [cAMP] is determined by the balance between AC and PDE activities (*Eq. 8*). Depression of V_{PDE} below V_{AC} will cause collapse of [cAMP] regulation, leading to a continuous accumulation of cAMP within cytosol. In both experiments and computer model simulations, quasi-steady-state [cAMP] levels were obtained even when the PDE activity was depressed by a saturating dose (>200 μM) of [IBMX]. This is because balancing V_{AC_t} with V_{PDE} was established with the IBMX-insensitive PDE fraction (~20% total PDE activities) under this extreme condition. To examine the robustness of the [cAMP] homeostasis in our model, the V_{AC_t} devoid of desensitization was compared with V_{PDE}, and the steady-state level of [cAMP] was defined by the intersection of V_{AC_t} with the [cAMP]-V_{PDE} curve in Fig. 8. When the V_{AC_t} was maximized at 500 nM [Ca^{2+}] using the saturating concentration of 100 nM [GLP-1], the equilibrium [cAMP] was obtained at ~115.7 μM with 20% V_{PDE} (grey sigmoidal curve) as indicated by the *arrow a*. This analysis determines that depression of V_{PDE} below ~14% will cause collapse of the [cAMP] homeostasis when V_{AC_t} was maximized. Under physiological conditions, the steady-state [cAMP] was maintained at 7.9 μM (*arrow b*) with intact V_{PDE} (black sigmoidal curve) even when AC was fully activated. The lower limit of [cAMP] in the absence of GLP-1 stimulation, on the other hand, is determined by the activity of the G protein-insensitive component of AC, and the [cAMP] was balanced at 1.4 μM (*arrow c*). It should be noted that this range of [cAMP] change (1.4~7.9 μM) well fits the dynamic range of the PKA activation ($K_{1/2}$ = ~3 μM). This analysis revealed that the intact PDE is highly capable of balancing V_{AC_t}, and thus we conclude that the system of [cAMP] regulation is quite robust in pancreatic β-cells. The delayed desensitization of the GLP-1 receptor (Fig. 4*D*) may further strengthen the robustness of the system.

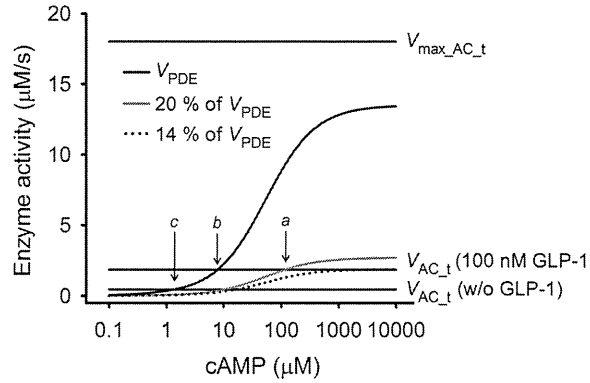

Fig. 8. Systems analysis on the robustness of GLP-1 signaling system in [cAMP] regulation. The black sigmoidal curve, the control V_{PDE} plotted as a function of [cAMP] at 500 nM [Ca^{2+}] (see *Eq. 13*). Grey curve, 20% of V_{PDE} under the presumptive presence of IBMX. Dotted curve, 14% V_{PDE}. The three horizontal lines from *top* to *bottom* indicate the sum of (V_{max_AC} + $V_{max\_AC\_G}$) and two levels of V_{AC_t} at 100 nM and 0 [GLP-1], respectively. To evaluate maximum possible levels of [cAMP] increase, the desensitization of the receptor was removed in this calculation. The *arrows a*, *b*, and *c* indicate intersections of V_{PDE} and V_{AC} curves. Note that [cAMP] can vary between the minimum level given by the *arrow c* and the maximum level given by the *arrow b* under the physiological condition. With 20% V_{PDE}, [cAMP] could increase to an extreme level (*arrow a*). Inhibition of V_{PDE} exceeding 14% would causes the "break-down" of the signaling system leading to a continuous [cAMP] accumulation, indicating that the intact PDE has an excessive capacity to balance against the production of cAMP by AC under physiological condition.

DISCUSSION

In the present study, a minimal model of GLP-1 receptor signal transduction was developed mostly based on experimental data reported in β-cells or related cell lines. The model successfully reconstructed the experimental findings of dynamic changes in [cAMP] during agonist stimulation in the absence or presence of IBMX at two representative levels of [Ca^{2+}] (Fig. 3). The model predicted the activity of cAMP effectors PKA and Epac during GLP-1 stimulation (Fig. 6). The simulation also demonstrated that the GLP-1 receptor desensitization kinetics applied to the model successfully explained the fast and very slow inactivation steps, which have significant effects on the decay kinetics of [cAMP] during continuous GLP-1 stimulation (Fig. 3) as well as reduced [cAMP] production after preconditioning of the receptor (Fig. 4 and Table 2). The cross talk between glucose- and GLP-1-dependent signal cascades in synergistic synthesis of cAMP was well reconstructed by incorporating the direct regulation of both AC and PDE by [Ca^{2+}] (Table 1). Models of the [Ca^{2+}]-dependent AC and PDE activities also elucidated the fractions of [Ca^{2+}]-sensitive components of these enzymes. Considering that [Ca^{2+}] is raised by [glucose] stimulation via the enhanced electrical activity of β-cells, the activation of GLP-1 signaling is a powerful amplifier for promoting the insulin release in the presence of stimulating concentrations of glucose.

The insulinotropic effect of the cAMP signal involves the activation of PKA and Epac, and subsequent modulation of ion channel functions (26, 31, 35, 41, 42, 57) and Ca^{2+} release from ER (27, 36, 64), in addition to their direct effects on the exocytotic machinery. The effects on ion channels, for example, include the enhancement of Ca^{2+} influx via L-type Ca^{2+} currents (26, 57) and inhibition of K^+ currents (26, 31, 35, 41, 42), which may in turn promote the insulin release via an increase in the membrane excitability. These comprehensive mechanisms of the insulinotropic effect of GLP-1 will be analyzed by incorporating the GLP-1 receptor signaling cascade model into appropriate whole β-cell models (24, 44) in the future.

In the present study, the distribution of [cAMP] within the cytosol of pancreatic β-cells was estimated (Fig. 7). It was suggested that the localization of cAMP beneath the surface membrane is insignificant even though production of cAMP is

limited at the submembrane space, while PDE-mediated degradation occurs diffusely within the cytosol. Our finding is, however, different from the localized cAMP microdomain observed in other cell types [cardiac myocytes (70) and HEK293 cells (61)]. The theoretical study by Oliveira et al. (47) demonstrated a large [cAMP] gradient (~5 μM) in HEK293 cells upon stimulation with PGE1. They concluded that the PDE4D activity enhanced by PKA-mediated phosphorylation was necessary and sufficient for generating the cAMP microdomain observed by Terrin et al. (61), and no physical barrier was required against the cAMP diffusion. If compared with our simulation, the cAMP diffusion constant used in their study was essentially the same magnitude as in our calculations. Interestingly, our diffusion model also generated a similar [cAMP] gradient of ~4 μM (Fig. 7*C*) when simulated using the V_{PDE} equivalent to that used in the Oliveira et al. (47). However, their V_{PDE} was much higher (~100 hold) than that determined by the model fitting to the published experimental data in the present study. If we adopt the higher PDE activity, the model failed to reconstruct experimental records of [cAMP] changes during GLP-1 stimulation. Our simulation results strongly suggest that the distribution of cAMP is homogeneous in pancreatic β-cells because of relatively low PDE activities. These results, however, do not necessarily exclude the possibility of a functional coupling among AC, PKA, and/or Epac and effecter proteins by AKAP near the membrane, which has been suggested in the heart and brain (12, 46). On the other hand, the rapid diffusion of [cAMP] could possibly be an essential factor in the GLP-1 receptor signaling for a proper modulation of insulin release, since PKA and Epac, the target proteins of cAMP, are widely distributed throughout the intracellular space (12, 40, 49). For activation of all these enzymes, the rapid access of cAMP might be critical to fulfill the basic needs of subsequent modulatory actions on ion channels on the surface and ER membrane as well as exocytotic machinery in concert within the entire intracellular space.

Sensitivity of the model to varying parameters. Athough [R] was estimated in a previous study (66), [G] has not yet been determined in pancreatic β-cells. In the present study, [G] was referred by Post et al. (50), who suggested the expression of G_s protein in large excess relative to β-adrenergic receptor in cardiac myocytes and hypothesized that this stoichiometry of [G] to [R] will be applicable to other G protein-coupled hormone receptor systems. We found that the EC_{50} of [GLP-1]-dependent [cAMP] accumulation is dependent on the agonist-induced [LRG] complex ([LRG] = [G]·[LR]/K_d), and thereby the EC_{50} can be adjusted by modifying either [G] or K_d of [G]-[LR] binding. Since both parameters have not been investigated in pancreatic β-cells, [GLP-1]-dependent [cAMP] accumulation was reconstructed by determining an appropreate K_d in the present study under the assumption that [G] is expressed to a similar extent as in the cardiac tissue (50). The fraction of [R_a] is one of signaling factors that have the strong influence on AC activities and thus [cAMP]. Under physiological conditions, [R_a] will largely fluctuate because of extensive desensitization (75% at the maximum, see Fig. 4*D*), which is expected to proceed during several hours of the meal digestion.

The maximum AC activity ($V_{max\_AC\_t} = V_{max\_AC} + V_{max\_AC\_G}$) is much larger than the V_{max} of PDE in our model. The lower AC activity under physiological conditions is mostly due to the low sensitivity of AC to G_αGTP in addition to the low [G_αGTP] production, even with a saturating [GLP-1] (see *Eq. 11*). Other modulatory factors of the AC activity, such as the dependencies on the substrate ATP and the Ca^{2+}-dependent inactivation, are nearly saturated with the physiological level of [ATP] and [Ca^{2+}]. Although Ca_xCaM-dependent activation of V_{AC_G} is pronounced with increasing [GLP-1], [cAMP] production becomes partially compensated by the parallel activation of PDE. More specifically, [cAMP] level balances at 7.61 μM under the stimulation with 10 nM GLP-1 at 500 nM [Ca^{2+}] without desensitization processes, whereas it increased to 8.61 μM when the component of Ca_xCaM-dependent activation of V_{PDE} was excluded from the model. The PDE component showing the high cAMP sensitivity (K_{mL}) also plays a subtle role in regulation [cAMP], whereas the low cAMP sensitivity (K_{mH}) component virtually fulfills the physiological role in cAMP hydrolysis in the present model.

Limitations. The kinetics of the simple sequential transition of desensitized receptors from R_{D1} to R_{D2} was modeled to describe the time course of the delayed recovery from slow inactivation (Fig. 4). Indeed, the reaction scheme for receptor desensitization (Fig. 1) well simulated both of the fast and very slow desensitization observed in experimental studies (see RESULTS). Up to date, it is clear that the phosphorylation of the GLP-1 receptor is the key desensitization step, whereas Widmann and colleagues (67) have shown that neither PKA nor PKC are involved in the process. The involvement of β-Arrestin2 and GRK5 was suggested by Jorgensen et al. (34), whereas it is still highly controversial since a different group demonstrated the desensitization was independent of β-Arrestin2 (59). The model scheme will need to be improved when the molecular mechanisms are established in future experimental studies. It may also be examined whether the activation of PDE through phosphorylation by PKA is responsible for a small fraction of the spontaneous decay of [cAMP], although the present study attributed the decay only to desensitization.

The active fractions of PKA as well as Epac1 and 2 were calculated by a use of biochemically determined K_d or $K_{1/2}$, half-maximal [cAMP] for the activation of these enzymes. However, especially for PKA activation, there has been obvious disagreement in published values of $K_{1/2}$, which vary over a nanomolar to micromolar range. It seems that the experimental $K_{1/2}$ is highly related to the concentration of enzyme used in biochemical investigations (7). $K_{1/2}$ was ~3 μM for more physiological concentration of the PKA isozyme II (400 nM), whereas it was significantly reduced to ~50 nM when tested on 1 nM holoenzyme. Indeed, other investigators (14) used low holoenzyme concentrations of 20~30 nM and obtained a $K_{1/2}$ of 98 nM and 540 nM for PKAI and PKAII, respectively. In the present study, PKA activities were calculated with $K_{1/2}$ of ~3 μM, yet, it may need to be reevaluated when more accurate experimental measurements of $K_{1/2}$ values as well as concentrations of PKA isozyme become available.

cAMP is distributed within a β-cell in forms of free cAMP and PKA or Epac-bound form (cAMP-PKA and cAMP-Epac). In the present study, however, [cAMP] was calculated neglecting [cAMP-PKA] and [cAMP-Epac]. If the total amount of cAMP is comparable to PKA and/or Epac, it will be necessary to consider [PKA] and/or [Epac] in calculating the concentration of unbound cAMP ($[cAMP]_{total}$ = [cAMP] + [cAMP-PKA] + [cAMP-Epac]). Similarly, the mass conservation should also be consid-

ered for [$G_\alpha GTP$] ([$G_\alpha GTP_{total}$] = [$G_\alpha GTP$] + [$G_\alpha GTP$-AC]) when [AC] is available. Since the amounts of PKA, Epac, and AC are not determined in β-cells, we excluded these conservation equations from the present model.

APPENDIX I

A) Parameters Determined in Published Experimental Studies

1) Parameters determined based on GLP-1 signaling system in pancreatic β-cell and a β-cell line

Total amount of receptor, [R_t] 0.00434 μM (Ref. 66)

Binding between [L] and [R] K_d = 0.004 μM (Refs. 43, 65)

2) Parameters determined by biochemical investigations

Total amount of Gs, [G_t] 2.83 μM (Ref. 50)

$G_\alpha GTP_{tot}$-dependent AC_G activation $K_{1/2}$ = 0.4 μM (Ref. 58)

ATP-dependent AC activity K_m = 1.03 mM (Ref. 13)

ATP-dependent AC_G activity K_m = 0.315 mM (Ref. 13)

Ca_xCaM-dependent AC_G activation $K_{1/2}$ = 0.348 μM (Ref. 21)

Ca^{2+}-dependent AC_G inhibition $K_{1/2i}$ = 75 μM (Ref. 21)

Ca_xCaM-dependent PDE activation $K_{1/2}$ = 0.348 μM (Ref. 68)

cAMP-dependent PKA activation K_d = 2.9μM,n_H = 1.4 (Ref.9)

cAMP-dependent Epac1 activation $K_{1/2}$ = 30 μM (Ref. 20)

cAMP-dependent Epac2 activation $K_{1/2}$ = 20 μM (Refs. 52, 63)

The kinetics for the activation and deactivation of Gs protein

$k5$ = 16 s-1, $k6$ = 1 s-1, $k7$ = 1, 200, 000 mM/s (Refs. 5, 56)

B) Parameters Determined in the Present Study by Fitting Specific Experimental Records or Measurements in References

Desensitization rate constants

$k1$ = 0.0025 s-1, $k2$ = 0.005833 s-1 (Fig. 3)

$k3$ = 0.0002833 s-1, $k4$ = 0.00005 s-1 (Fig. 4 and Table 3)

AC and PDE activities (Figs. 3 and 6 and Table 2)

$$V_{AC}V_{max\_AC} = 0.0006173 \text{ mM/s}$$

$$V_{AC\_G}V_{max\_AC\_G} = 0.01738 \text{ mM/s}$$

$$f_{Cd\_AC} = 0.6$$

V_{PDE}

$$V_{max\_PDE} = 0.015 \text{ mM/s}$$

$$f_{Cd\_PDE} = 0.2$$

$$K_{ml} = 0.4148 \text{ μM}, K_{mH} = 53.98 \text{ μM}$$

$$f = 0.012$$

C) Parameters Determined in the Present Study by Fitting the Overall Model Scheme to Experimental Records or Measurements In References

Binding between [G] and [LR] K_d = 0.372 μM (Ref. 66)

ACKNOWLEDGMENTS

The authors acknowledge insightful discussions with Dr. T. Powell and valuable suggestions made by Dr. G. G. Holz. The authors also thank Drs. T. Shimayoshi, C. Cha, Y. Himeno, and other members in the Biosimulation Project for helpful discussion as well as technical supports.

GRANTS

This work was supported by the Regional Innovation Cluster Program (Biomedical Cluster Kansai) of the Ministry of Education, Culture, Sports, Science and Technology, Japan and a Grant-In-Aid for Scientific Research from the Ministry of Education, Culture, Sports, Science and Technology, Japan.

DISCLOSURES

No conflicts of interest, financial or otherwise, are declared by the author(s).

REFERENCES

1. **Ahmad M, Abdel-Wahab YH, Tate R, Flatt PR, Pyne NJ, Furman BL.** Effect of type-selective inhibitors on cyclic nucleotide phosphodiesterase activity and insulin secretion in the clonal insulin secreting cell line BRIN-BD11. *Br J Pharmacol* 129: 1228–1234, 2000.
2. **Arava Y, Adamsky K, Ezerzer C, Ablamunits V, Walker MD.** Specific gene expression in pancreatic beta-cells: cloning and characterization of differentially expressed genes. *Diabetes* 48: 552–556, 1999.
3. **Baggio LL, Kim JG, Drucker DJ.** Chronic exposure to GLP-1R agonists promotes homologous GLP-1 receptor desensitization in vitro but does not attenuate GLP-1R-dependent glucose homeostasis in vivo. *Diabetes* 53, *Suppl* 3: S205–S214, 2004.
4. **Bender AT, Beavo JA.** Cyclic nucleotide phosphodiesterases: molecular regulation to clinical use. *Pharmacol Rev* 58: 488–520, 2006.
5. **Brandt DR, Ross EM.** Catecholamine-stimulated GTPase cycle. Multiple sites of regulation by beta-adrenergic receptor and Mg^{2+} studied in reconstituted receptor-Gs vesicles. *J Biol Chem* 261: 1656–1664, 1986.
6. **Chen C, Nakamura T, Koutalos Y.** Cyclic AMP diffusion coefficient in frog olfactory cilia. *Biophys J* 76: 2861–2867, 1999.
7. **Christensen AE, Selheim F, de RJ, Dremier S, Schwede F, Dao KK, Martinez A, Maenhaut C, Bos JL, Genieser HG, Doskeland SO.** cAMP analog mapping of Epac1 and cAMP kinase. Discriminating analogs demonstrate that Epac and cAMP kinase act synergistically to promote PC-12 cell neurite extension. *J Biol Chem* 278: 35394–35402, 2003.
8. **Cooper DM.** Regulation and organization of adenylyl cyclases and cAMP. *Biochem J* 375: 517–529, 2003.
9. **Dao KK, Teigen K, Kopperud R, Hodneland E, Schwede F, Christensen AE, Martinez A, Doskeland SO.** Epac1 and cAMP-dependent protein kinase holoenzyme have similar cAMP affinity, but their cAMP domains have distinct structural features and cyclic nucleotide recognition. *J Biol Chem* 281: 21500–21511, 2006.
10. **Dean PM.** Ultrastructural morphometry of the pancreatic cell. *Diabetologia* 9: 115–119, 1973.
11. **Delmeire D, Flamez D, Hinke SA, Cali JJ, Pipeleers D, Schuit F.** Type VIII adenylyl cyclase in rat beta cells: coincidence signal detector/generator for glucose and GLP-1. *Diabetologia* 46: 1383–1393, 2003.
12. **Dessauer CW.** Adenylyl cyclase–A-kinase anchoring protein complexes: the next dimension in cAMP signaling. *Mol Pharmacol* 76: 935–941, 2009.
13. **Dessauer CW, Scully TT, Gilman AG.** Interactions of forskolin and ATP with the cytosolic domains of mammalian adenylyl cyclase. *J Biol Chem* 272: 22272–22277, 1997.
14. **Dostmann WR, Taylor SS.** Identifying the molecular switches that determine whether (Rp)-cAMPS functions as an antagonist or an agonist in the activation of cAMP-dependent protein kinase I. *Biochemistry* 30: 8710–8716, 1991.
15. **Dov A, Abramovitch E, Warwar N, Nesher R.** Diminished phosphodiesterase-8B potentiates biphasic insulin response to glucose. *Endocrinology* 149: 741–748, 2008.
16. **Drucker DJ.** The biology of incretin hormones. *Cell Metab* 3: 153–165, 2006.
17. **Drucker DJ, Philippe J, Mojsov S, Chick WL, Habener JF.** Glucagon-like peptide I stimulates insulin gene expression and increases cyclic AMP levels in a rat islet cell line. *Proc Natl Acad Sci USA* 84: 3434–3438, 1987.
18. **Dryselius S, Grapengiesser E, Hellman B, Gylfe E.** Voltage-dependent entry and generation of slow Ca^{2+} oscillations in glucose-stimulated pancreatic β-cells. *Am J Physiol Endocrinol Metab* 276: E512–E518, 1999.
19. **Dyachok O, Isakov Y, Sagetorp J, Tengholm A.** Oscillations of cyclic AMP in hormone-stimulated insulin-secreting beta-cells. *Nature* 439: 349–352, 2006.
20. **Enserink JM, Christensen AE, de RJ, van TM, Schwede F, Genieser HG, Doskeland SO, Blank JL, Bos JL.** A novel Epac-specific cAMP

analogue demonstrates independent regulation of Rap1 and ERK. *Nat Cell Biol* 4: 901–906, 2002.
21. **Fagan KA, Mahey R, Cooper DM.** Functional co-localization of transfected Ca(2+)-stimulable adenylyl cyclases with capacitative Ca^{2+} entry sites. *J Biol Chem* 271: 12438–12444, 1996.
22. **Frace AM, Mery PF, Fischmeister R, Hartzell HC.** Rate-limiting steps in the beta-adrenergic stimulation of cardiac calcium current. *J Gen Physiol* 101: 337–353, 1993.
23. **Fridlyand LE, Harbeck MC, Roe MW, Philipson LH.** Regulation of cAMP dynamics by Ca^{2+} and G protein-coupled receptors in the pancreatic β-cell: a computational approach. *Am J Physiol Cell Physiol* 293: C1924–C1933, 2007.
24. **Fridlyand LE, Tamarina N, Philipson LH.** Modeling of Ca^{2+} flux in pancreatic β-cells: role of the plasma membrane and intracellular stores. *Am J Physiol Endocrinol Metab* 285: E138–E154, 2003.
25. **Gilon P, Ravier MA, Jonas JC, Henquin JC.** Control mechanisms of the oscillations of insulin secretion in vitro and in vivo. *Diabetes* 51, *Suppl* 1: S144–S151, 2002.
26. **Gromada J, Bokvist K, Ding WG, Holst JJ, Nielsen JH, Rorsman P.** Glucagon-like peptide 1 (7–36) amide stimulates exocytosis in human pancreatic beta-cells by both proximal and distal regulatory steps in stimulus-secretion coupling. *Diabetes* 47: 57–65, 1998.
27. **Gromada J, Brock B, Schmitz O, Rorsman P.** Glucagon-like peptide-1: regulation of insulin secretion and therapeutic potential. *Basic Clin Pharmacol Toxicol* 95: 252–262, 2004.
28. **Han P, Werber J, Surana M, Fleischer N, Michaeli T.** The calcium/calmodulin-dependent phosphodiesterase PDE1C down-regulates glucose-induced insulin secretion. *J Biol Chem* 274: 22337–22344, 1999.
29. **Hanoune J, Defer N.** Regulation and role of adenylyl cyclase isoforms. *Annu Rev Pharmacol Toxicol* 41: 145–174, 2001.
29a. **Harvey, RD.** How uniform is cAMP signaling? Focus on "Systems analysis of GLP-1 receptor signaling in pancretic β-cells." *Am J Physiol Cell Physiol* (July 20, 2011). doi:10.1152/ajpcell.00245.2011.
30. **Holz GG.** Epac: A new cAMP-binding protein in support of glucagon-like peptide-1 receptor-mediated signal transduction in the pancreatic beta-cell. *Diabetes* 53: 5–13, 2004.
31. **Holz GG, Kuhtreiber WM, Habener JF.** Pancreatic beta-cells are rendered glucose-competent by the insulinotropic hormone glucagon-like peptide-1(7–37). *Nature* 361: 362–365, 1993.
32. **Huang RC, Gillette R.** Kinetic analysis of cAMP-activated Na^+ current in the molluscan neuron. A diffusion-reaction model. *J Gen Physiol* 98: 835–848, 1991.
33. **Idevall-Hagren O, Barg S, Gylfe E, Tengholm A.** cAMP mediators of pulsatile insulin secretion from glucose-stimulated single beta-cells. *J Biol Chem* 285: 23007–23018, 2010.
34. **Jorgensen R, Martini L, Schwartz TW, Elling CE.** Characterization of glucagon-like peptide-1 receptor beta-arrestin 2 interaction: a high-affinity receptor phenotype. *Mol Endocrinol* 19: 812–823, 2005.
35. **Kang G, Chepurny OG, Malester B, Rindler MJ, Rehmann H, Bos JL, Schwede F, Coetzee WA, Holz GG.** cAMP sensor Epac as a determinant of ATP-sensitive potassium channel activity in human pancreatic beta cells and rat INS-1 cells. *J Physiol* 573: 595–609, 2006.
36. **Kang G, Chepurny OG, Rindler MJ, Collis L, Chepurny Z, Li WH, Harbeck M, Roe MW, Holz GG.** A cAMP and Ca^{2+} coincidence detector in support of Ca^{2+}-induced Ca^{2+} release in mouse pancreatic beta cells. *J Physiol* 566: 173–188, 2005.
37. **Kashima Y, Miki T, Shibasaki T, Ozaki N, Miyazaki M, Yano H, Seino S.** Critical role of cAMP-GEFII–Rim2 complex in incretin-potentiated insulin secretion. *J Biol Chem* 276: 46046–46053, 2001.
38. **Landa LR Jr, Harbeck M, Kaihara K, Chepurny O, Kitiphongspattana K, Graf O, Nikolaev VO, Lohse MJ, Holz GG, Roe MW.** Interplay of Ca^{2+} and cAMP signaling in the insulin-secreting MIN6 beta-cell line. *J Biol Chem* 280: 31294–31302, 2005.
39. **Lester LB, Langeberg LK, Scott JD.** Anchoring of protein kinase A facilitates hormone-mediated insulin secretion. *Proc Natl Acad Sci USA* 94: 14942–14947, 1997.
40. **Li Y, Asuri S, Rebhun JF, Castro AF, Paranavitana NC, Quilliam LA.** The RAP1 guanine nucleotide exchange factor Epac2 couples cyclic AMP and Ras signals at the plasma membrane. *J Biol Chem* 281: 2506–2514, 2006.
41. **Light PE, Manning Fox JE, Riedel MJ, Wheeler MB.** Glucagon-like peptide-1 inhibits pancreatic ATP-sensitive potassium channels via a protein kinase A- and ADP-dependent mechanism. *Mol Endocrinol* 16: 2135–2144, 2002.
42. **MacDonald PE, Salapatek AM, Wheeler MB.** Glucagon-like peptide-1 receptor activation antagonizes voltage-dependent repolarizing K(+) currents in beta-cells: a possible glucose-dependent insulinotropic mechanism. *Diabetes* 51, *Suppl* 3: S443–S447, 2002.
43. **Mathi SK, Chan Y, Li X, Wheeler MB.** Scanning of the glucagon-like peptide-1 receptor localizes G protein-activating determinants primarily to the N terminus of the third intracellular loop. *Mol Endocrinol* 11: 424–432, 1997.
44. **Meyer-Hermann ME.** The electrophysiology of the beta-cell based on single transmembrane protein characteristics. *Biophys J* 93: 2952–2968, 2007.
45. **Nauck MA, Heimesaat MM, Orskov C, Holst JJ, Ebert R, Creutzfeldt W.** Preserved incretin activity of glucagon-like peptide 1 [7–36 amide] but not of synthetic human gastric inhibitory polypeptide in patients with type-2 diabetes mellitus. *J Clin Invest* 91: 301–307, 1993.
46. **Nijholt IM, Dolga AM, Ostroveanu A, Luiten PG, Schmidt M, Eisel UL.** Neuronal AKAP150 coordinates PKA and Epac-mediated PKB/Akt phosphorylation. *Cell Signal* 20: 1715–1724, 2008.
47. **Oliveira RF, Terrin A, Di BG, Cannon RC, Koh W, Kim M, Zaccolo M, Blackwell KT.** The role of type 4 phosphodiesterases in generating microdomains of cAMP: large scale stochastic simulations. *PLoS One* 5: e11725, 2010.
48. **Pipeleers D.** The biosociology of pancreatic B cells. *Diabetologia* 30: 277–291, 1987.
49. **Ponsioen B, Gloerich M, Ritsma L, Rehmann H, Bos JL, Jalink K.** Direct spatial control of Epac1 by cyclic AMP. *Mol Cell Biol* 29: 2521–2531, 2009.
50. **Post SR, Hilal-Dandan R, Urasawa K, Brunton LL, Insel PA.** Quantification of signalling components and amplification in the beta-adrenergic-receptor-adenylate cyclase pathway in isolated adult rat ventricular myocytes. *Biochem J* 311: 75–80, 1995.
51. **Pyne NJ, Furman BL.** Cyclic nucleotide phosphodiesterases in pancreatic islets. *Diabetologia* 46: 1179–1189, 2003.
52. **Rehmann H, Arias-Palomo E, Hadders MA, Schwede F, Llorca O, Bos JL.** Structure of Epac2 in complex with a cyclic AMP analogue and RAP1B. *Nature* 455: 124–127, 2008.
53. **Roger B, Papin J, Vacher P, Raoux M, Mulot A, Dubois M, Kerr-Conte J, Voy BH, Pattou F, Charpentier G, Jonas JC, Moustaid-Moussa N, Lang J.** Adenylyl cyclase 8 is central to glucagon-like peptide 1 signalling and effects of chronically elevated glucose in rat and human pancreatic beta cells. *Diabetologia* 54: 390–402, 2011.
54. **Sams DJ, Montague W.** The role of adenosine 3′:5′-cyclic monophosphate in the regulation of insulin release. Properties of islet-cell adenosine 3′:5′-cyclic monophosphate phosphodiesterase. *Biochem J* 129: 945–952, 1972.
55. **Santos RM, Rosario LM, Nadal A, Garcia-Sancho J, Soria B, Valdeolmillos M.** Widespread synchronous $[Ca^{2+}]_i$ oscillations due to bursting electrical activity in single pancreatic islets. *Pflügers Arch* 418: 417–422, 1991.
56. **Saucerman JJ, Brunton LL, Michailova AP, McCulloch AD.** Modeling beta-adrenergic control of cardiac myocyte contractility in silico. *J Biol Chem* 278: 47997–48003, 2003.
57. **Suga S, Kanno T, Dobashi Y, Wakui M.** GLP-1 (7–36) amide activates L-type Ca^{2+} channels of pancreatic B-cells through c-AMP signaling. *Jpn J Physiol* 47, *Suppl* 1: S13–S14, 1997.
58. **Sunahara RK, Dessauer CW, Whisnant RE, Kleuss C, Gilman AG.** Interaction of Gsalpha with the cytosolic domains of mammalian adenylyl cyclase. *J Biol Chem* 272: 22265–22271, 1997.
59. **Syme CA, Zhang L, Bisello A.** Caveolin-1 regulates cellular trafficking and function of the glucagon-like Peptide 1 receptor. *Mol Endocrinol* 20: 3400–3411, 2006.
60. **Tengholm A, Gylfe E.** Oscillatory control of insulin secretion. *Mol Cell Endocrinol* 297: 58–72, 2009.
61. **Terrin A, Di BG, Pertegato V, Cheung YF, Baillie G, Lynch MJ, Elvassore N, Prinz A, Herberg FW, Houslay MD, Zaccolo M.** PGE(1) stimulation of HEK293 cells generates multiple contiguous domains with different [cAMP]: role of compartmentalized phosphodiesterases. *J Cell Biol* 175: 441–451, 2006.
62. **Thorens B.** Expression cloning of the pancreatic beta cell receptor for the gluco-incretin hormone glucagon-like peptide 1. *Proc Natl Acad Sci USA* 89: 8641–8645, 1992.
63. **Tsalkova T, Blumenthal DK, Mei FC, White MA, Cheng X.** Mechanism of Epac activation: structural and functional analyses of Epac2 hinge

mutants with constitutive and reduced activities. *J Biol Chem* 284: 23644–23651, 2009.

64. **Tsuboi T, da S, X, Holz GG, Jouaville LS, Thomas AP, Rutter GA.** Glucagon-like peptide-1 mobilizes intracellular Ca^{2+} and stimulates mitochondrial ATP synthesis in pancreatic MIN6 beta-cells. *Biochem J* 369: 287–299, 2003.
65. **Wheeler MB, Lu M, Dillon JS, Leng XH, Chen C, Boyd AE, III.** Functional expression of the rat glucagon-like peptide-I receptor, evidence for coupling to both adenylyl cyclase and phospholipase-C. *Endocrinology* 133: 57–62, 1993.
66. **Widmann C, Burki E, Dolci W, Thorens B.** Signal transduction by the cloned glucagon-like peptide-1 receptor: comparison with signaling by the endogenous receptors of beta cell lines. *Mol Pharmacol* 45: 1029–1035, 1994.
67. **Widmann C, Dolci W, Thorens B.** Desensitization and phosphorylation of the glucagon-like peptide-1 (GLP-1) receptor by GLP-1 and 4-phorbol 12-myristate 13-acetate. *Mol Endocrinol* 10: 62–75, 1996.
68. **Yan C, Zhao AZ, Bentley JK, Beavo JA.** The calmodulin-dependent phosphodiesterase gene PDE1C encodes several functionally different splice variants in a tissue-specific manner. *J Biol Chem* 271: 25699–25706, 1996.
69. **Yu X, Byrne JH, Baxter DA.** Modeling interactions between electrical activity and second-messenger cascades in Aplysia neuron R15. *J Neurophysiol* 91: 2297–2311, 2004.
70. **Zaccolo M, Pozzan T.** Discrete microdomains with high concentration of cAMP in stimulated rat neonatal cardiac myocytes. *Science* 295: 1711–1715, 2002.

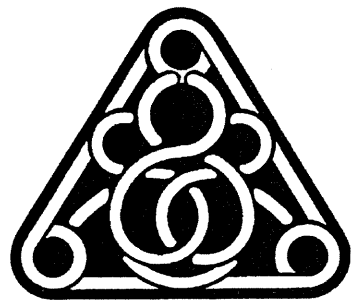

Analysis of factors influencing postprandial C-peptide levels in Japanese patients with type 2 diabetes: Comparison with C-peptide levels after glucagon load

Shogo Funakoshi[1], Shimpei Fujimoto[1]*, Akihiro Hamasaki[1], Hideya Fujiwara[1], Yoshihito Fujita[1], Kaori Ikeda[1], Shiho Takahara[1], Yutaka Seino[2], Nobuya Inagaki[1]

ABSTRACT

Aims/Introduction: Postprandial serum C-peptide levels are readily determined in clinical practice and have a good correlation with serum C-peptide levels after glucagon load; the measurement is often used as an index of endogenous insulin secretion. However, the factors affecting postprandial serum C-peptide levels remain to be evaluated.

Materials and Methods: To investigate the clinical factors affecting postprandial serum C-peptide, 2-h postprandial C-peptide levels after breakfast (PPCPR) were analyzed retrospectively for comparison with glucagon-stimulated C-peptide (CPR-6min) levels measured during hospital admission in 273 Japanese patients with type 2 diabetes.

Results: Multiple regression analysis showed that years from diagnosis, body mass index (BMI) and HbA_{1c} were the major independent variables predicting PPCPR ($R^2 = 0.315$). HbA_{1c} was a major factor predicting PPCPR, but did not predict CPR-6min. In addition, HbA_{1c} was negatively correlated with PPCPR ($r = -0.410$, $P < 0.0001$) and PPCPR/CPR-6min ($r = -0.313$, $P < 0.0001$).

Conclusions: PPCPR was correlated with common factors predicting CPR, including years from diagnosis and BMI, but also was negatively correlated with HbA_{1c}, a unique factor. These results show that chronic elevation of the glucose level might impair endogenous insulin secretion after meal load, but might have little effect on endogenous insulin secretion after glucagon load.

(J Diabetes Invest, doi: 10.1111/j.2040-1124.2011.00126.x, 2011)

KEY WORDS: C-peptide, Meal load, HbA_{1c}

INTRODUCTION

Type 2 diabetes is a heterogeneous disease characterized by insulin resistance and defective insulin secretion[1], and is progressive in that the mode of therapy must be altered over the decades of diabetes; diet and exercise therapy alone might be adequate initially, but secondary oral hypoglycemic agent (OHA) treatment and insulin treatment are eventually required[2,3]. This is, at least in part, as a result of progressive loss of pancreatic β-cell function. The results of the United Kingdom Progressive Diabetes Study (UKPDS) show that pancreatic β-cell function (%β), assessed by Homeostasis Model Assessment (HOMA) in patients allocated to diet or OHA decreased approximately 25% in 5 years[4]. In addition, a decline in endogenous insulin secretion over more than several decades of diabetes in patients including insulin-treated patients was observed in a cross-sectional study[5].

Determination of fasting serum C-peptide level and stimulated serum C-peptide level by intravenous glucagon is used widely to assess endogenous insulin secretory reserves[6–9], and the utility of the indices using C-peptide level in choosing insulin therapy has been shown[10]. The postprandial serum C-peptide level can easily be measured in clinical practice and has a good correlation with the serum C-peptide level after glucagon load[11]; it is often used as an index of endogenous insulin secretion, and can be used for both non-insulin-treated and insulin-treated patients[11–13]. Duration of diabetes and body mass index (BMI) are the major factors in serum fasting and glucagon-stimulated C-peptide levels[5,14], but the factors affecting postprandial serum C-peptide levels remain to be evaluated.

In the present study of Japanese patients with type 2 diabetes, to evaluate the clinical factors affecting postprandial serum C-peptide by cross-sectional study, 2-h postprandial C-peptide levels after breakfast were analyzed and compared with glucagon-stimulated C-peptide levels.

[1]Department of Diabetes and Clinical Nutrition, Graduate School of Medicine, Kyoto University, Kyoto, and [2]Kansai Electric Power Hospital, Osaka, Japan
*Corresponding author. Shimpei Fujimoto Tel.: +81-75-751-3560
Fax: +81-75-751-4244 E-mail address: fujimoto@metab.kuhp.kyoto-u.ac.jp
Received 18 January 2011; revised 8 March 2011; accepted 23 March 2011

SUBJECTS AND METHODS

Subjects

A total of 388 Japanese patients with type 2 diabetes who were admitted to Kyoto University Hospital between 1997 and 2002 for poor glycemic control were enrolled in the study. Patients with pancreatic or liver disease, taking diabetogenic medications, pregnant or with serum creatinine ≥1.3 mg/dL were excluded from the study. Type 2 diabetes mellitus was diagnosed based on the criteria of the American Diabetes Association (ADA)[15]. Patients with serum creatinine ≥1.3 mg/dL were excluded, as serum C-peptide immunoreactivity (CPR) is elevated by decreased renal function[16]. Of these patients, 115 were excluded as a result of incomplete clinical examinations and the remaining 273 patients, including patients without diabetic medication, oral hypoglycemic agent-treated patients and insulin-treated patients, were analyzed. The clinical profiles of the patients are shown in Table 1.

Methods

On the first day in hospital, medical history, physical examination and laboratory evaluation including glycosylated hemoglobin were carried out. HbA_{1c} was measured using high performance liquid chromatography (HA-8180; Arcray, Kyoto, Japan). The HbA_{1c} (%) value was estimated as a National Glycohemoglobin Standardization Program (NGSP) equivalent (%) calculated by the formula HbA_{1c} (%) = HbA_{1c} (Japan Diabetes Society [JDS]) (%) + 0.4%, considering the relational expression of HbA_{1c} (JDS) (%) measured by the previous Japanese standard substance and measurement methods and HbA_{1c} (NGSP)[17]. β-Cell function was evaluated within 1 week after an overnight fast by measuring fasting CPR (FCPR), CPR 6min after intravenous injection of 1 mg glucagon (CPR-6min)[6] and postprandial CPR. Serum CPR was measured by radioimmunoassay (Daiichi III; Daiichi Radioisotope Laboratories, Osaka, Japan). Postprandial CPR 2 h after breakfast (PPCPR) was determined. The meal at breakfast was prescribed as nutritional therapy according to the treatment guide for diabetes of the JDS[18], which included 516.6 ± 67.7 kcal (mean ± SD) energy consisting of 49% carbohydrate, 16% protein and 35% fat. In patients taking OHA, medication was stopped for measurement of CPR, but was maintained until 1 day before to prevent hyperglycemia during the test[5]. Plasma glucose was measured by the glucose oxidase method.

The study protocol was approved by the ethics committee of Kyoto University.

Table 1 | Clinical profiles of patients

No. patients	273
Male/female	158/115
Age (years)	61.2 ± 12.2
Years from diagnosis	9.6 ± 9.6
Systolic blood pressure (mmHg)	121.8 ± 12.9
Diastolic blood pressure (mmHg)	73.6 ± 9.6
BMI (kg/m^2)	23.9 ± 3.7
HbA_{1c} at admission (%)	9.7 ± 2.0
sCre (mg/dL)	0.69 ± 0.18
Glucagon load: FPG/PG-6min (mg/dL)	164.1 ± 47.9/180.6 ± 49.1
Glucagon load: FCPR/CPR-6min (ng/mL)	1.80 ± 0.97/3.83 ± 1.76
Meal load: FPG/PPPG (mg/dL)	167.0 ± 54.8/271.5 ± 83.5
Meal load: FCPR/PPCPR (ng/mL)	1.76 ± 0.94/4.87 ± 2.41

BMI, body mass index; CPR-6min, C-peptide immunoreactivity 6 min after intravenous injection of 1 mg glucagon; FCPR, fasting CPR; FPG, fasting plasma glucose; OHA, oral hypoglycemic agents; PG-6min, plasma glucose 6 min after glucagon load; PPCPR, postprandial CPR; PPPG, postprandial plasma glucose; sCre, serum creatinine.

Statistical Analysis

Statistical analysis was carried out with the Stat View 5.0 system (SAS institute Inc., Cary, NC, USA). Data are presented as mean ± SD, unless otherwise noted. The relationship between the parametric clinical data and CPR values was investigated by Pearson's analysis. The relationship between the non-parametric clinical data and CPR values was investigated by Spearman's analysis. Clinical parameters among three groups were compared by analysis of variance (ANOVA). For comparison of two groups, Scheffé's test was carried out. *P*-values < 0.05 were considered statistically significant.

RESULTS

Simple correlation coefficients between FCPR, CPR-6min and PPCPR, and measures of variables (age, years from diagnosis, sex, BMI, systolic and diastolic blood pressure, HbA_{1c}, serum creatinine and plasma glucose [PG]) were calculated and are shown in Table 2. Years from diagnosis and BMI were significantly correlated with all three measures of CPR. PG and HbA_{1c} were significantly correlated with PPCPR ($P < 0.0001$, $r = -0.410$), but not with CPR-6min (Figure 1).

Stepwise multiple regression analysis was carried out using the independent variables in Table 2 to predict CPR as a dependent variable (Table 3). FCPR was independently predicted by years from diagnosis, BMI and serum creatinine, accounting for 22.4% of the variability of FCPR. CPR-6min was independently predicted by years from diagnosis and BMI, accounting for 17.9% of the variability of the dependent variables. PPCPR was independently predicted by years from diagnosis, BMI and HbA_{1c}, accounting for 31.5% of the variability of the dependent variables. Thus, HbA_{1c} is an important independent variable predicting PPCPR, but not FCPR or CPR-6min.

Because HbA_{1c} might be involved in decreased PPCPR, the clinical data among three groups of increased HbA_{1c} (≤8.5%, 8.6–10.3%, ≥10.4%) were compared, as shown in Table 4. Although there was no significant difference among these groups in FCPR and CPR-6min, PPCRP was significantly reduced with increasing levels of HbA_{1c}. CPR-6min was significantly correlated with PPCPR ($P < 0.0001$, $r = 0.564$, PPCPR = 0.774 × CPR-6min + 1.913; Figure 2a). PPCPR was correlated with CPR-6min in each tertile group of HbA_{1c} ($HbA_{1c} \leq 8.5$:

Table 2 | *P*-values and *r*-values of correlation between C-peptide immunoreactivity and measures of variables

	FCPR (ng/mL)	CPR-6min (ng/mL)	PPCPR (ng/mL)
Age (years)	0.4257 (ND)	0.0456 (−0.121)	0.3896 (ND)
Years from diagnosis	0.0024 (−0.182)	<0.0001 (−0.246)	0.0007 (−0.205)
Sex	0.0709 (ND)	0.1879 (ND)	0.8321 (ND)
BMI (kg/m^2)	<0.0001 (0.435)	<0.0001 (0.367)	<0.0001 (0.311)
Systolic blood pressure (mmHg)	0.5551 (ND)	0.9388 (ND)	0.0865 (ND)
Diastolic blood pressure (mmHg)	0.5739 (ND)	0.0327 (0.130)	0.0705 (ND)
HbA_{1c} (%)	0.0443 (−0.122)	0.1507 (ND)	<0.0001 (−0.410)
sCre (mg/dL)	0.0104 (0.155)	0.1641 (ND)	0.0140 (0.148)
FPG (mg/dL)	0.3764 (ND)	ND	ND
PG-6min (mg/dL)	ND	0.7333 (ND)	ND
PPPG (mg/dL)	ND	ND	<0.0001 (−0.285)

All correlations except correlations between sex and C-peptide immunoreactivity (CPR) were analyzed by Pearson's analysis. Correlations between sex and CPR were analyzed by Spearman's analysis. *P*-values are shown. In parenthesis, *r*-values are shown.
BMI, body mass index; CPR-6min, C-peptide immunoreactivity 6 min after intravenous injection of 1 mg glucagon; FCPR, fasting CPR; FPG, fasting plasma glucose; ND, not determined; PG-6min, plasma glucose 6 min after glucagon load; PPCPR: postprandial CPR; PPPG: postprandial plasma glucose; sCre: serum creatinine.

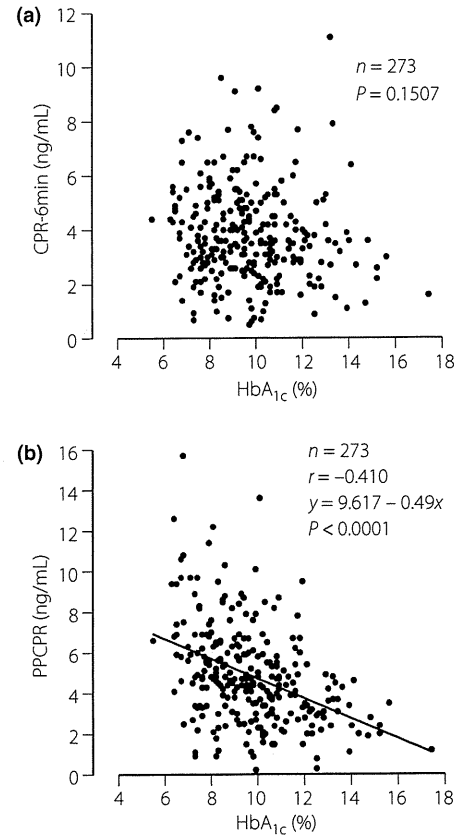

Figure 1 | The relationship between HbA_{1c} and (a) C-peptide immunoreactivity 6 min after intravenous injection of 1 mg glucagon (CPR-6min) and (b) 2-h postprandial C-peptide levels after breakfast (PPCPR).

$P < 0.0001$, $r = 0.595$, $y = 2.159 + 0.970x$, $n = 90$; $8.6\% \leq HbA_{1c} \leq 10.3\%$: $P < 0.0001$, $r = 0.674$, $y = 1.587 + 0.829x$, $n = 92$; $10.4\% \leq HbA_{1c}$: $P < 0.0001$, $r = 0.494$, $y = 2.091 + 0.482x$, $n = 91$). Because the higher HbA_{1c} group was distributed mainly below the regression line of total patients and the lower HbA_{1c} group above the line in the scattergram, and the increase in PPCPR per CPR-6min in the regression line of each tertile group was lower in the higher HbA_{1c} group, we examined the correlation between the ratio of PPCPR to CPR-6min (PPCPR/CPR-6min) and HbA_{1c}. PPCPR/CPR-6min was negatively correlated with HbA_{1c} ($P < 0.0001$, $r = -0.313$; Figure 2b).

DISCUSSION

In the present study, HbA_{1c} was negatively correlated with PPCPR, but not with FCPR or CPR-6min, which suggests that chronic elevation of the glucose level might impair endogenous insulin secretion after a meal load.

Although meal load is not equivalent to glucose load, as it contains nutrients other than carbohydrates that modulate glucose-induced insulin secretion, elevated glucose in plasma might play an important role in meal-stimulated insulin secretion. Indeed, the plasma glucose level after a meal load was increased considerably to more than 100 mg/dL in average. In contrast, the increment of glucose after glucagon load was only approximately 15 mg/dL, indicating a small contribution of glucose elevation to increased insulin secretion by glucagon loading.

Because HbA_{1c} was positively correlated with PPPG in the present study ($P < 0.0001$, $r = 0.570$), HbA_{1c} reflects postprandial glucose level. In simple correlation, both HbA_{1c} and PPPG were significantly correlated with PPCPR; whereas in stepwise regression analysis, HbA_{1c} was important to predict PPCPR, but PPPG was not. In addition, in simple correlation to PPCPR, the *r*-value for HbA_{1c} (0.410) was larger compared with that for PPPG (0.285; Table 2). These results show that PPCPR is more strongly affected by chronic elevation of glucose levels than by transient elevation of glucose levels.

Multiple regression analysis showed that years from diagnosis, BMI and HbA_{1c} were the major independent variables predicting PPCPR. This shows that years from diagnosis and BMI are common major factors predicting CPR. In contrast, HbA_{1c} was the major factor predicting PPCPR, but not FCPR or CPR-6min, and was negatively correlated with PPCPR. We hypothesized that CPR-6min reflects reserve capacity of endogenous insulin secretion independent of glycemic control and that PPCPR is predicted by a fundamental factor independent of glycemic control and by a variable factor dependent of glycemic control. CPR-6min predicted 31.8% of the variability of PPCPR as shown in Figure 2a. When a regression model using CPR-6min

Table 3 | Stepwise multiple regression analysis for predictors of C-peptide immunoreactivity

	F-value	Partial regression coefficient	Standard partial regression coefficient	R^2 (*R*)
FCPR (ng/mL)				
Years from diagnosis	9.4	−0.017	−0.170	0.224 (0.473)
BMI (kg/m^2)	55.2	0.108	0.406	
sCre (mg/dL)	7.3	0.823	0.149	
CPR-6min (ng/mL)				
Years from diagnosis	14.6	−0.039	−0.214	0.179 (0.423)
BMI (kg/m^2)	38.9	0.170	0.349	
PPCPR (ng/mL)				
Years from diagnosis	23.4	−0.063	−0.252	0.315 (0.561)
BMI (kg/m^2)	27.5	0.178	0.270	
HbA_{1c} (%)	68.7	−0.516	−0.431	

BMI, body mass index; CPR-6min, C-peptide immunoreactivity 6 min after intravenous injection of 1 mg glucagon; FCPR, fasting CPR; PPCPR, postprandial CPR; sCre, serum creatinine.

Table 4 | Comparison of clinical characteristics and clinical profile among groups according to HbA_{1c} at admission

Groups (HbA_{1c} at admission)	I (≤8.5%)	II (8.6–10.3%)	III (≥10.4%)	*P*
No. patients	90	92	91	
HbA_{1c} (%)	7.6 ± 0.1	9.5 ± 0.1*†	12.0 ± 0.1*†	<0.0001
Sex (male/female)	53/37	55/37	50/41	
Age (years)	64.2 ± 1.2	61.6 ± 1.3	57.6 ± 1.3*	0.0011
BMI (kg/m^2)	24.2 ± 0.3	24.1 ± 0.4	23.5 ± 0.4	0.3579
Years from diagnosis	11.7 ± 1.2	9.7 ± 0.8	7.4 ± 0.8*	0.0088
bSBP (mmHg)	122.9 ± 1.4	120.6 ± 1.3	121.3 ± 1.4	0.4746
DBP (mmHg)	72.9 ± 1.2	72.7 ± 1.0	75.3 ± 0.9	0.1302
sCre (mg/dL)	0.74 ± 0.02	0.70 ± 0.02	0.63 ± 0.02*†	<0.0001
FPG (mg/dL)	134.2 ± 3.7	163.4 ± 3.9*	195.0 ± 5.4*†	<0.0001
PG-6min (mg/dL)	152.4 ± 3.9	178.7 ± 4.0*	211.1 ± 5.6*†	<0.0001
PPPG (mg/dL)	223.3 ± 6.4	268.2 ± 7.7*	323.7 ± 8.9*†	<0.0001
FCPR (ng/mL)	1.92 ± 0.10	1.84 ± 0.10	1.66 ± 0.11	0.2004
CPR-6min (ng/mL)	3.85 ± 0.18	3.97 ± 0.19	3.66 ± 0.18	0.5467
PPCPR (ng/mL)	5.90 ± 0.29	4.88 ± 0.24*	3.86 ± 0.18*†	<0.0001

Data are presented as mean ± SE.
*$P < 0.01$ vs group I, †$P < 0.01$ vs group II.
BMI, body mass index; CPR-6min, C-peptide immunoreactivity 6 min after intravenous injection of 1 mg glucagon; DBP, diastolic blood pressure; FCPR, fasting CPR; FPG, fasting plasma glucose; PG-6min, plasma glucose 6 min after glucagon load; PPCPR, postprandial CPR; PPPG, postprandial plasma glucose; SBP, systolic blood pressure; sCre, serum creatinine. FPG and FCPR are values when meal load was carried out.

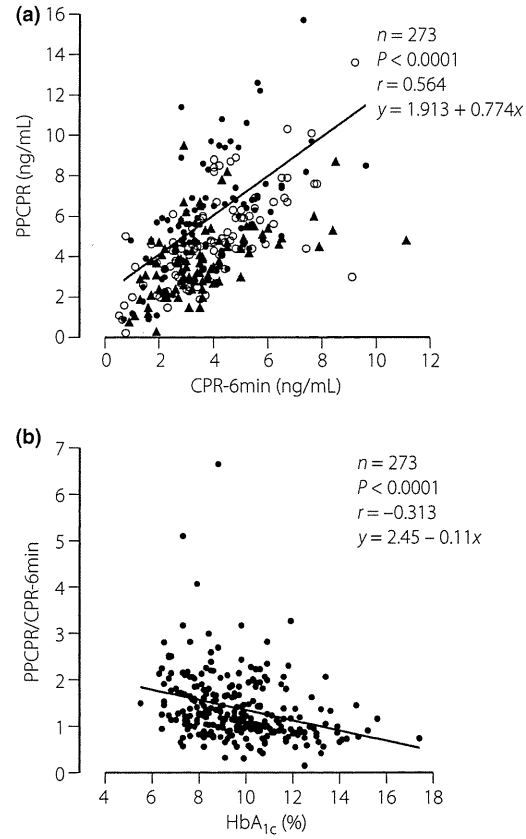

Figure 2 | Relationship between (a) C-peptide immunoreactivity 6 min after intravenous injection of 1 mg glucagon (CPR-6min) and 2-h postprandial C-peptide levels after breakfast (PPCPR) and (b) PPCPR/CPR-6min and HbA_{1c}. Black circles, $HbA_{1c} \leq 8.5\%$; white circles, $8.6\% \leq HbA_{1c} \leq 10.3\%$, black triangles, $10.4\% \leq HbA_{1c}$

and HbA_{1c} as independent variables to predict PPCPR as a dependent variable was used, CPR-6min and HbA_{1c} predicted 44.9% of the variability of PPCPR ($P < 0.0001$, $R = 0.670$, PPCPR = 6.286 + 0.730 × CPR-6min − 0.434 × HbA_{1c}). The addition of HbA_{1c} as an independent variable increased the prediction of the variability of PPCPR by 13.1%. In the present study, PPCPR/CPR-6min was used as a putative index of variability dependent of glycemic control and was found to be correlated with HbA_{1c} in the present study (Figure 2b). Furthermore, improvement of glycemic control by treatment ameliorates the CPR response after oral glucose load[19–21]. In addition, the CPR response after glucagon load is affected little by treatment to improve hyperglycemia and it is not correlated with the CPR response after oral glucose load before treatment, whereas it is well-correlated with improved CPR response after oral glucose load after treatment[21]. Reversible impairment of endogenous insulin response after glucose load is explained by glucose toxicity, in which chronic hyperglycemia deteriorates meal-induced and glucose-induced insulin secretion and insulin-sensitive glucose disposal[22]. Therefore, the chronic high glucose

